Dine-Fischler-Srednicki-Zhitnitsky-type axions and where to find them

Johannes Diehl[1],[*] and Emmanouil Koutsangelas[2],[1],[†]

[1]*Max-Planck-Institut für Physik, Föhringer Ring 6, 80805 München, Germany*
[2]*Arnold Sommerfeld Center, Ludwig-Maximilians-Universität München,*
Theresienstraße 37, 80333 München, Germany

We systematically calculate the axion-photon coupling for nonminimal Dine-Fischler-Srednicki-Zhitnitsky (DFSZ) models. Thereby, we can classify every calculated model and study the resulting distributions, relevant for axion experiments like haloscopes, helioscopes, or light-shining-through-a-wall experiments. By adding more than one additional Higgs doublet, these nonminimal DFSZ models extend the viable axion parameter space and lead to a large range of axion-photon couplings. We find couplings almost 3 orders of magnitude larger than the ones of the minimal models. Most of the possible axion-photon couplings, however, lie in the vicinity of the values dictated by the minimal models. We quantify this by introducing a theoretical prior probability distribution for DFSZ-type axions and giving 68% and 95% lower bounds as well as two-sided bands. We compare our results for the DFSZ axion-photon coupling distributions with the Kim-Shifman-Vainshtein-Zakharov case, for which a similar analysis has been conducted. Both display similar values as well as a very specific pattern. In order to identify preferred models, we discuss the role of flavor changing neutral currents and the domain wall problem as possible selection criteria. It is possible to construct a large number of nonminimal DFSZ models with a domain wall number of unity, thereby avoiding the domain wall problem. This subset also has a significantly enhanced axion-photon coupling compared to the minimal DFSZ models.

I. INTRODUCTION

The strong CP problem remains one of the biggest puzzles of particle physics. While it is usually expressed as the inexplicable smallness of the CP violating θ parameter, i.e., $\theta < 10^{-10}$ [1], it is in fact a vacuum selection problem rooted in the nontrivial vacuum structure of QCD [2]. What makes this "small value" problem special is that within the Standard Model (SM), quantum corrections to θ are many orders of magnitude below the experimental bound [3] (unlike the Higgs mass for instance) so that it is not really a problem for θ to be that small. In this sense, any explanation for the smallness of θ is just theoretically motivated.

However, in recent years, it has been pointed out that when quantum gravity is taken into account, consistency relations are imposed that exclude any type of (meta)stable de Sitter vacua [4–6]. Since any theory with $\theta \neq 0$ is of

de Sitter-type, this reduces the number of viable vacua to exactly one: the CP conserving vacuum at $\theta = 0$. This does not only promote the strong CP problem to a real problem, but it also makes a mechanism that results in $\theta = 0$ a necessity [7,8].

Such a mechanism is given by the Peccei-Quinn (PQ) solution, which essentially introduces a nonlinearly realized $U(1)_{PQ}$ that is anomalous with respect to QCD [9,10]. The crucial anomaly condition can be expressed as the nonconservation of the PQ current, namely

$$\partial_\mu J^\mu_{PQ} = N \frac{\alpha_s}{4\pi} G\tilde{G} + E \frac{\alpha}{4\pi} F\tilde{F}, \qquad (1)$$

where the electromagnetic anomaly, which in general is also present, is added. In this expression, G, F denote the color and electromagnetic field strength tensors, $\tilde{G}$, $\tilde{F}$ their duals, α_s, α their associated fine-structure constants, and N, E the corresponding anomaly coefficients. The PQ mechanism solves the strong CP problem by making the θ parameter unobservable as it gets relaxed to zero by the pseudo-Goldstone boson of the PQ symmetry, the axion [11,12].

The PQ solution is special in the sense that it predicts a new light pseudoscalar particle. However, it does not specify the axion low-energy couplings that depend on the UV physics [13]. The low-energy effective theory is thus not sufficient, and UV models are needed to make

[*]diehl@mpp.mpg.de
[†]emi@mpp.mpg.de

concrete predictions about the couplings of the axion. This is usually achieved by the two large classes of invisible axion models, the Dine-Fischler-Srednicki-Zhitnitsky (DFSZ)-type [14,15] and Kim-Shifman-Vainshtein-Zakharov (KSVZ)-type models [16,17]. The former adds Higgs singlets and doublets to the SM, while the latter adds Higgs singlets and heavy quarks (for a review, see [18]). Even though the minimal models of each type, adding only one Higgs doublet or one quark of arbitrary representation, define benchmark models, in principle, there is a plethora of nonminimal models. An identification of all these models and systematic approach that allows one to extract a prediction from all these models at the same time would be desirable. The goal of this work is to do exactly this for the DFSZ-type axions.

We achieve this by exploiting the unique property of the axion-photon coupling: Its UV physics are fully encoded in the ratio between the electromagnetic and the QCD anomaly coefficients [13],

$$g_{a\gamma} = \frac{\alpha}{2\pi f_a}\left[\frac{E}{N} - 1.92(4)\right] \equiv \frac{\alpha}{2\pi f_a}\mathcal{C}_{a\gamma}, \qquad (2)$$

where f_a is the axion decay constant, and by $\mathcal{C}_{a\gamma}$, we denote the dimensionless part.

Because of the nature of anomalies, this ratio does not depend on unknown vacuum expectation values (VEVs) or mixing angles but only on the representation of the fields. For the DFSZ-type models, this comes down to fixing the PQ charges of the SM fermions that are not free but determined by consistency and phenomenology conditions [18]. Systematically solving the associated linear system of equations (LSE) allows us to calculate the anomaly ratio and thus, the axion-photon coupling for a large number of DFSZ-type models.

In addition to calculating the anomaly ratios for a large number of DFSZ-type models, we are able to count how many different models lead to the same anomaly ratio. We then use this notion of multiplicity to allocate a certain probability to each anomaly ratio. From analyzing the resulting distributions, we are able to extract several interesting conclusions for the axion experimental program. One of our key observations is that the values dictated by the minimal DFSZ models, namely $E/N = 2/3$ and $E/N = 8/3$, are statistically favored for DFSZ-type theories, even though for a larger number of Higgs doublets, many more possible values for the anomaly ratio can exist. While this confirms the potential experimental importance of these values, on the other hand, we argue that a nonobservation at these values still leaves a significant amount of the axion parameter space viable. We quantify this statement by defining an axion band as well as lower $g_{a\gamma}$ bounds.

A similar analysis has already been done for the KSVZ-type axion: The identification and classification is described in [19], while the statistical analysis is reported in [20]. Furthermore, in [19], a part is dedicated to DFSZ-type axions. There, by estimating the maximal possible anomaly ratio, the authors argue that the majority of realistic DFSZ-type models lie in the same window as the preferred KSVZ-type ones. With our work, we are not only able to give a more precise value of the maximal possible anomaly ratio, which turns out to be higher than the previous estimate, but to also perform a detailed comparison between the two classes, which allows us to better understand their relation.

The paper is organized as follows. To begin with, in Sec. II, we review DFSZ-type models where we put the focus on the determination of the PQ charges. Moreover, we discuss potential phenomenological selection criteria and give a general procedure on how to determine all possible anomaly ratios and their multiplicities for a given number of Higgs doublets. In Sec. III, we apply this approach to theories with three to nine Higgs doublets. We discuss arising problems for a high number of doublets and compare our results with the KSVZ-type models. Next, Sec. IV discusses experimental implications by estimating necessary sensitivities for axion searches. Lastly, in Sec. V, we summarize our results and give an outlook.

II. DFSZ-TYPE AXION MODELS

In the DFSZ-type of models, the fermionic fields of the SM are charged under the PQ symmetry. This requires one to enlarge the scalar content of the SM by one singlet and at least one additional Higgs doublet. The additional doublets are required for the PQ mechanism to make the PQ symmetry anomalous with respect to QCD. The singlet is introduced to render the axion invisible by decoupling the PQ scale from the electroweak scale [14,15].

The anomaly of the PQ current only depends on the difference between the PQ charges of left- and right-handed fermions. For simplicity, we set the PQ charges of the left-handed fermions to zero. This leaves us with the charges of the right-handed ones, which we denote as $\chi_{u_i}, \chi_{d_i}, \chi_{e_i}$ with i being a generation index. Regarding the neutrinos, the situation is somewhat special. While the left-handed neutrino is not directly contributing to the anomaly ratio E/N, it could be contributing indirectly if a right-handed neutrino was present in the theory. Since it is currently unknown if the neutrino masses are realized via the type-I seesaw mechanism, which requires the introduction of the right-handed neutrinos, we exclude the neutrinos in our analysis by setting their PQ charge to zero in accordance with the other left-handed fermions.

In the following, we denote the DFSZ-type models as DFSZ_{n_D}, where n_D is the total number of doublets. In this terminology, the original models, which represent the minimal versions, become DFSZ_2-I and DFSZ_2-II with $E/N = 2/3$ and $E/N = 8/3$, respectively.

A. Identifying the axion

Let us for concreteness consider a DFSZ_{n_D} model with $n_D \leq 9$ and begin by fixing the Yukawa sector. In order to exhaust the maximum freedom of the PQ charges, we consider a Yukawa sector where each right-handed fermion couples to only one doublet. This makes it reasonable to denote the doublets as H^{u_i}, H^{d_i}, H^{e_i}, and the singlet as S. The Yukawa sector then takes the form,

$$\mathcal{L} \supset -y_{ij}^u H^{u_i} \bar{Q}_L^i u_R^j - y_{ij}^d H^{d_i} \bar{Q}_L^i d_R^j - y_{ij}^e H^{e_i} \bar{E}_L^i e_R^j + \text{H.c.} \tag{3}$$

For $n_D = 9$, each right-handed fermion couples to a different doublet, while for $n_D < 9$, some fermions have to couple to the same doublet. This form of the Yukawa sector automatically fixes the weak hypercharge of the doublets to be

$$-Y_{H^{u_i}} = Y_{H^{d_i}} = Y_{H^{e_i}} = \frac{1}{2}. \tag{4}$$

In principle, several doublets can couple to the same right-handed fermion. We ignore this issue for now and come back to it in Sec. II C.

Next, the standard kinetic term for each scalar is invariant under a $U(1)^{n_D+1}$ symmetry. This symmetry must be explicitly broken down to $U(1)_{\mathrm{PQ}} \times U(1)_Y$ for the PQ current to be well-defined and to avoid Goldstone bosons with decay constants of electroweak scale order. With this requirement in mind, we split the potential into two parts,

$$V = V_{\mathrm{moduli}} + V_{\mathrm{eb}}. \tag{5}$$

The first term, V_{moduli}, only consists of the modulus of each scalar or the modulus of two doublets and hence, does not break any of the global $U(1)$ groups explicitly. In contrast, V_{eb} consists of terms that all break the $U(1)^{n_D+1}$ symmetry explicitly. Since this symmetry must be broken down to $U(1)_{\mathrm{PQ}} \times U(1)_Y$, the number of terms in V_{eb} required is $n_D - 1$.

Being a proper scalar potential, in this basis, all scalar fields develop VEVs v_f, where the index $f = u_i, d_i, e_i, S$ is introduced for compactness. Expanding around these VEVs yields,

$$H_{d_i} \supset \frac{v_{d_i}}{\sqrt{2}} e^{i\frac{a_{d_i}}{v_{d_i}}} \begin{pmatrix} 0 \\ 1 \end{pmatrix}, \qquad H_{u_i} \supset \frac{v_{u_i}}{\sqrt{2}} e^{i\frac{a_{u_i}}{v_{u_i}}} \begin{pmatrix} 1 \\ 0 \end{pmatrix},$$

$$H_{e_i} \supset \frac{v_{e_i}}{\sqrt{2}} e^{i\frac{a_{e_i}}{v_{e_i}}} \begin{pmatrix} 0 \\ 1 \end{pmatrix}, \qquad S \supset \frac{v_S}{\sqrt{2}} e^{i\frac{a_S}{v_S}}, \tag{6}$$

where any angular degrees of freedom not containing the axion are neglected. Each angular mode a_f transforms under a PQ transformation as $a_f \to a_f + \kappa_f \chi_f v_f$, where the

χ_f denote the PQ charges, and the κ_f are constants. The corresponding PQ current after spontaneous symmetry breaking is then

$$J_\mu^{\mathrm{PQ}}\Big|_a \supset -\chi_S S^\dagger i\partial^\mu S - \sum_{f\backslash S} \chi_f H_f^\dagger i\partial^\mu H_f + \text{H.c.}$$

$$= \sum_f \chi_f v_f \partial_\mu a_f. \tag{7}$$

By requiring $J_\mu^{\mathrm{PQ}}\big|_a = v_a \partial_\mu a$ and $a \to a + \kappa v_a$ under the PQ transformation, the axion field is defined as

$$a = \frac{1}{v_a} \sum_f \chi_f v_f a_f, \qquad v_a^2 = \sum_f \chi_f^2 v_f^2. \tag{8}$$

Thus, in the DFSZ-type models, the axion is a linear combination of all scalar angular modes.

With the axion identified, the low-energy theory is constructed in the standard way. By inverting Eq. (8), the scalar angular modes can be expressed in terms of the axion. Since we are only interested in the terms including the axion, this comes down to the replacement,

$$\frac{a_f}{v_f} \to \chi_f \frac{a}{v_a}. \tag{9}$$

The Lagrangian can then be brought to a more convenient form by a field-dependent chiral redefinition of the fermion fields,

$$f \to \exp\left(-i\gamma_5 \chi_f \frac{a}{2v_a}\right) f. \tag{10}$$

This redefinition removes the axion from the fermion mass terms, but due to the invariance of the kinetic terms, it induces derivative couplings to the fermions. In addition, since in general, the PQ current is anomalous with respect to QCD and electromagnetism, anomalous couplings to the gluons and the photons are induced,

$$\delta\mathcal{L}_{\mathrm{anomalous}} = N \frac{a}{v_a} \frac{g_s^2}{16\pi^2} G\tilde{G} + E \frac{a}{v_a} \frac{g^2}{16\pi^2} F\tilde{F}$$

$$= \frac{a}{f_a} \frac{g_s^2}{32\pi^2} G\tilde{G} + \frac{E}{N} \frac{a}{f_a} \frac{g^2}{32\pi^2} F\tilde{F}, \tag{11}$$

where the axion decay constant $f_a \equiv v_a/2N$ is introduced in the second equality. The canonically normalized axion-photon interaction is defined via

$$\mathcal{L}_{a\gamma} = \frac{1}{4} g_{a\gamma} F\tilde{F}, \tag{12}$$

so taking into account next-to-leading-order chiral corrections [21] results in the axion-photon coupling given in Eq. (2).

Since in the models under consideration all representations except the PQ charges are known, the ratio between the electromagnetic and color anomaly coefficients can conveniently be written as [19]

$$\frac{E}{N} = \frac{\sum_i \frac{4}{3}\chi_{u_i} + \frac{1}{3}\chi_{d_i} + \chi_{e_j}}{\frac{1}{2}\sum_i \chi_{u_i} + \chi_{d_i}} = \frac{2}{3} + 2\frac{\sum_i \chi_{u_i} + \chi_{e_i}}{\sum_i \chi_{u_i} + \chi_{d_i}}. \quad (13)$$

Hence, the determination of the anomaly ratio, and thus, the axion-photon coupling comes down to the determination of the PQ charges, which we turn to now. For further details regarding the DFSZ axion and an explicit construction of the original DFSZ models, see [18].

B. The PQ charges

The key point regarding the PQ charges is that the explicit breaking of the $U(1)^{n_D+1}$ symmetry into $U(1)_{PQ} \times U(1)_Y$ must respect the following conditions [18]:

(1) Orthogonality between the PQ current J_μ^{PQ} and the weak hypercharge current J_μ^Y.

(2) Invariance under PQ symmetry.

(3) Well-definiteness of domain wall (DW) number N_{DW}.

Consequently, the PQ charges are not arbitrary but interrelated by the $n_D + 1$ relations following from these conditions. Solving the resulting LSE then yields a solution for all PQ charges.

To begin with, the orthogonality requirement between the PQ current defined in Eq. (7) and the weak hypercharge current $J_\mu^Y|_a = \sum_f Y_f v_f \partial_\mu a_f$ implies

$$\sum \chi_f Y_f v_f^2 = 0. \quad (14)$$

From this relation, one can immediately see that, in general, the PQ charges are not integer numbers. This can also be concluded by the fact that $U(1)_{PQ}$ is not compact.

For the PQ invariance, we divide the $n_D - 1$ terms of V_{eb} into two kinds, namely terms consisting of two doublets and two times the singlet, or terms with four doublets. We denote them symbolically as *HHSS* and *HHHH* in the following. We restrict ourselves to renormalizable terms so that higher orders in the scalars do not appear. Since the axion must be rendered invisible, there must be at least one term of the form *HHSS*. The form of the other $n_D - 2$ terms is then in principle free.

It is crucial that the terms in V_{eb} are chosen such that they give rise to linearly independent conditions. In other words, we require V_{eb} to have enough terms to render the system exactly solvable and not underdetermined nor overdetermined. Underdetermined systems do not explicitly break enough of the $U(1)^{n_D+1}$ symmetry, hence, giving rise to

undesired massless states. Overdetermined systems, on the other hand, are inconsistent (we come back to systems with linearly dependent terms in Sec. II C).

It should also briefly be mentioned that all resulting sets of PQ charges with $N = 0$ do not solve the strong *CP* problem and should thus be discarded.

With the conditions of orthogonality and PQ invariance, it is reasonable to solve for all PQ charges in terms of χ_S, which is otherwise unconstrained as a singlet. The value of χ_S is irrelevant for the anomaly ratio since it cancels in the ratio. Hence, for a set of terms chosen in V_{eb}, we can express all PQ charges in terms of χ_S and calculate the anomaly ratio. This is the key message of this subsection.

However, there are quantities in which χ_S does not cancel. One of these quantities is the DW number. Since there is a potential cosmological problem associated with higher DW numbers that we discuss in Sec. II D, it is useful to fix χ_S as well. In particular, it turns out that in theories where the axion is a linear combination of fields, a consistency condition on χ_S follows from the DW number N_{DW} being integer valued.

In the low-energy regime, the QCD anomaly induces a periodic potential to the axion. Let us for illustrative purpose take the potential induced by instantons in the dilute instanton gas approximation [22,23],

$$V(\theta) = \Lambda_{QCD}^4 \left[1 - \cos\left(2N \frac{a}{v_a} \right) \right], \quad (15)$$

where we expressed the axion decay constant $f_a = v_a/2N$ in terms of v_a. The periodicity of the potential results in discrete vacua, and the number of these vacua in a single 2π-loop is the DW number N_{DW}, which can be read off to be $N_{DW} = 2N$. In the language of symmetries, this potential explicitly breaks the original $U(1)_{PQ}$ down to the discrete group $\mathbb{Z}_{N_{DW}}$, under which, the axion transforms as $a \to a + 2\pi n f_a$ with $n \in \mathbb{Z}$. The DW number is encoded in this transformation, and it is given by the n that results in a single loop of circumference $2\pi v_a$, yielding again $N_{DW} = 2N$.

However, there is a caveat in theories where the axion is a linear combination of angular modes a_f [24]. There, each angular mode also has a residual cyclic symmetry from its explicit breaking, namely $a_f \to a_f + 2\pi n_f v_f$, where $n_f \in \mathbb{Z}$. To take these residual symmetries into account, we apply them on both sides of the first equation in Eq. (8) and read off the DW number as defined in the previous paragraph,

$$N_{DW} = 2N \frac{\sum n_f \chi_f v_f^2}{\sum \chi_f^2 v_f^2}. \quad (16)$$

For the DW number to be integer, we must demand the fraction in this expression to be integer (as it turns out, this can be, without loss of generality, chosen to be one).

The simplest way is given by $n_f = \chi_f$, which would require the compactness of each $U(1)$ and is thus very restrictive. A less restrictive alternative can be found by plugging in the orthogonality condition into the numerator and the denominator of the fraction to remove one of the v_f and then comparing terms with the same v_f^2. Let us for simplicity perform this in DFSZ$_2$, where $f = u, d, S$, and require the fraction to be one. We find

$$n_S = \chi_S, \tag{17}$$

$$n_u + n_d = \chi_u + \chi_d = 2\chi_S, \tag{18}$$

where, in the second equality, we used the PQ invariance from the unique $V_{\rm eb}$ term, i.e., $H_u H_d S S$. We see that the residual cyclic symmetries of the underlying angular modes result in the condition $\chi_S \in \mathbb{Z}$ in the minimal DFSZ model.

Repeating this procedure for larger numbers of doublets, we find that Eq. (17) is always present and that there are more relations of the type of Eq. (18). These relations imply that for the DW number to be integer, χ_S and certain combinations of PQ charges must be integer. In particular, $2N = \sum_i \chi_{u_i} + \chi_{d_i}$ and $\sum_i \chi_{u_i} + \chi_{e_i}$ are such combinations. The key difference for nonminimal models is that fulfilling all appearing conditions is more restrictive than in the minimal case, for instance, requiring the minimal value of χ_S to be integer and larger than one.

To summarize, we see that in theories where the axion is a linear combination of fields, the DW number can again be written as $N_{\rm DW} = 2N$ but with the premise that the fraction in Eq. (16) is one. This additional condition comes down to the requirement of χ_S being integer but not necessarily one. For the sake of the discussion in Sec. II D, it is useful to fix χ_S to its minimal possible value. Thus, we conveniently define the DW number as

$$N_{\rm DW} = \text{min positive integer}\{2N\}, \tag{19}$$

and use this definition for the remainder of this work.

C. Multiplicity

The way the PQ charges are fixed, as described in the previous subsection, makes the calculation of all possible anomaly ratios straightforward, at least in principle. However, when it comes to defining a notion of *multiplicity*, further specification is needed because of potential overcounting of models. When constructing models, the standard mantra is to include all possible terms compatible with the given symmetries. If for some reason, terms are not included at tree level, without protection from an underlying symmetry, these terms will be generated at higher orders.

Regarding $V_{\rm eb}$, this has the implication that potentials that give rise to the *same* PQ charges should not be considered different since they can simply be added. This can be understood in the language of conditions and LSEs. The construction described in Sec. II B required $n_D - 1$ terms in the explicit breaking potential. Less terms would result in undesired Goldstone bosons, while too many independent terms result in overdetermined systems that have $\chi_f = 0$ for all f and thus, do not solve the strong CP problem. However, one can add more and more terms to the potential that give rise to redundant conditions. These are exactly the potentials that have the same solution of the underlying LSE, i.e., that have the same PQ charges.

This reasoning also has consequences for the Yukawa sector. The construction we described starts by coupling a single doublet to each right-handed fermion, but, in principle, several doublets can couple to the same right-handed fermion. For this reason, we complete the Yukawa sector *a posteriori* for each set of possible PQ charges. For instance, such a completion of the Yukawa sector could look as follows. If we find as a possible solution for some LSE that $\chi_{d1} = \chi_{e1}$, then the Yukawa sector for that solution becomes

$$y_{1j}^d H^{d_1} \bar{Q}_L^1 d_R^j \rightarrow (y_{1j}^d H^{d_1} + \tilde{y}_{1j}^d H^{e_1}) \bar{Q}_L^1 d_R^j,$$
$$y_{1j}^e H^{e_1} \bar{E}_L^i e_R^j \rightarrow (\tilde{y}_{1j}^e H^{d_1} + y_{1j}^e H^{e_1}) \bar{E}_L^i e_R^j. \tag{20}$$

This guarantees that all possible Yukawa terms compatible with a given solution are included (such as cross-couplings where for instance up-type doublets couple to down-type fermions). In addition, since every set of PQ charges is unique after adding the potentials, the Yukawa sector with all compatible couplings is uniquely determined, and no additional multiplicities need to be taken into account.

Adding the potentials and completing the Yukawa sectors for a specific set of PQ charges specify one model for the counting of the multiplicity. The last step is then to calculate the anomaly ratio for each model and count its multiplicity, which completes the construction procedure.

D. Selection criteria

With the models specified, the question arises if it is possible to impose (phenomenological) selection criteria in order to extract preferred axion models.

In the KSVZ-type models, which add additional heavy quarks and one singlet scalar to the SM, all of the selection criteria follow from the presence of the new fermions [19]. For instance, if the new quarks are too heavy and too long lived, they are subject to strong Big Bang nucleosynthesis and cosmic microwave background bounds. Moreover, since their mass is related to f_a, the concrete value of f_a plays an important role. Lastly, the presence of additional quarks dramatically affects the running of the QCD coupling constant, potentially spoiling asymptotic freedom and leading to Landau poles below the Planck scale. All these bounds are not present in the DFSZ case,

so we are not discussing them further (see [19] or [20] for a detailed discussion).

Next, let us briefly discuss the aspects that are present in both types of invisible axion models, starting with the DW problem. As mentioned in Sec. II B, at temperatures of order of the QCD scale $T \sim \Lambda_{\text{QCD}}$, nonperturbative QCD effects generate an effective potential [25]. This potential explicitly breaks the original PQ symmetry down to the discrete group $\mathbb{Z}_{N_{\text{DW}}}$, which is then spontaneously broken by one of the vacua. This leads to the formation of DWs that attach themselves to the cosmic strings (from the spontaneous breaking of the PQ symmetry at $T \sim f_a$) and form string-wall systems. For $N_{\text{DW}} > 1$, the strings stabilize the DWs so that these would dominate the energy density of the universe—this is the DW problem [26] (see [27] for a review). Thus, one could impose $N_{\text{DW}} = 1$ as a selection criterion for axion models.

However, there are several ways to avoid the DW problem. First of all, it is not present when the PQ symmetry is broken during or before inflation since then no DWs form inside our Hubble sphere. In the scenario when the PQ symmetry is broken after inflation, it is also possible that the symmetry is not restored at high T, thus avoiding the production of strings and walls [28]. Alternatively, by embedding the discrete subgroup into a continuous group, the different vacua become related via symmetry transformations, which results in an effective DW number of unity [29]. Because of these known solutions, we do not consider $N_{\text{DW}} = 1$ to have a sufficient level of generality to represent a necessary selection criterion for our main analysis. Nevertheless, we do calculate the DW number for DFSZ_3 to DFSZ_7, demonstrate the influence of this selection criterion, and compare with the KSVZ case in Sec. IV B.

Furthermore, staying in the same category of aspects that are present for both types of invisible axion models, the presence of additional Higgs doublets alters the running of the electroweak gauge coupling. In particular, the maximal case of $n_D = 9$ seems to improve unification with respect to the SM, but the resulting unification scale of $\Lambda_{\text{GUT}} \sim 10^{13}$ GeV leads to unacceptable fast proton decay. For this reason and for the sake of a better comparability with the KSVZ case, we consider improvement of unification not applicable as a selection criterion. In addition, it should also be mentioned that for $n_D \sim 50$, asymptotic freedom is spoiled, and a Landau Pole appears below the Planck scale, providing a hard upper limit on the number of doublets [19].

Let us finally turn to an aspect that is only present in the DFSZ-type models, namely the general feature of multi-Higgs doublet models to include flavor-changing neutral currents (FCNCs). Since FCNCs are subject to strong experimental constraints [30], they could, in principle, severely reduce the number of viable DFSZ-type models. However, similar to the DW problem, there are known ways to avoid these FCNC (see [31] for a review):

(i) *Natural flavor conservation:* The easiest way to avoid FCNCs is to impose the Weinberg-Glashow-Paschos condition [32,33], which requires all right-handed fermions of a given electric charge to couple to only one of the doublets. Imposing this condition effectively sets several Yukawa couplings to zero, which for $n_D > 3$, results in $n_D - 3$ decoupled Higgs doublets. Hence, for DFSZ-type models as we have defined them in the beginning of this section, natural flavor conservation is only possible for $n_D \leq 3$.

(ii) *Flavor alignment:* A less restrictive possibility is to impose an alignment condition, i.e., requiring the Yukawa matrices of each right-handed fermion to be proportional to one Yukawa matrix. All Yukawa matrices are then simultaneously diagonalized in the fermion mass eigenbasis, yielding no FCNC at tree level [34–36].

(iii) *Mass matrix ansätze:* Another possibility is to take the Yukawa matrices to have a specific texture in flavor space. This allows viable SM mass and mixing phenomenology and sufficient suppression of the tree-level FCNCs [37].

Natural flavor conservation and mass matrix ansätze are usually implemented by imposing (discrete) symmetries, which also protect the flavor structure from quantum corrections. However, imposing additional symmetries on the scalar potential spoils the so-called decoupling property of general multi-Higgs doublet models [38]. This means that the new scalar cannot have arbitrary large masses, resulting in potentially significant deviations from the measured SM couplings. So, in order to avoid FCNC using these solutions, it would be necessary to systematically determine which of our models have discrete symmetries that avoid FCNC and, at the same time, allow for a decoupling limit. Due to the large number of models and the lack of a catalogue of possible symmetries for $n_D > 3$ [31], such an analysis goes beyond the scope of this work.

Flavor alignment, on the other hand, is usually assumed without an underlying symmetry protection. While this preserves the decoupling limit of general multi-Higgs doublet models, it leaves the flavor structure vulnerable to quantum corrections. However, due to residual flavor symmetries, the induced misalignment is sufficiently small [39].

All in all, in the DFSZ case, we find desirable features for specific models but no selection criteria with a sufficient level of generality.

Lastly, we want to mention that, in principle, it is possible to enlarge the definition of DFSZ-type axions to include more singlets or more than $n_D = 9$ doublets, which do not couple to the SM fermions. From the point of view of possible axion-photon couplings, this does not change Eq. (13); however, it allows one to obtain very large PQ charges [19,40]. We do not consider these models in this paper and stick with the more narrow definition of

TABLE I.   Resulting PQ conditions from quadrilinears, constructed from corresponding bilinears. The lower triangle ("−") is not to be counted because the order of the bilinears does not matter. The terms "x" are not to be counted because they are Hermitian to a term that has already been counted, and the potential by definition has to include all Hermitian conjugated terms. Terms with "o" produce only trivial conditions. We are left with nine distinct quadrilinears, which produce six unique conditions.

	$(H_u H_d)$	$(H_u H_e)$	$(H_d H_e^\dagger)$	$(H_u H_d)^\dagger$	$(H_u H_e)^\dagger$	$(H_d H_e^\dagger)^\dagger$
$(H_u H_d)$	$2\chi_u + 2\chi_d = 0$	$2\chi_u + \chi_d + \chi_e = 0$	$\chi_u + 2\chi_d - \chi_e = 0$	o	$\chi_d - \chi_e = 0$	$\chi_u + \chi_e = 0$
$(H_u H_e)$	−	$2\chi_u + 2\chi_e = 0$	$\chi_u + \chi_d = 0$	x	o	$\chi_u - \chi_d + 2\chi_e = 0$
$(H_d H_e^\dagger)$	−	−	$2\chi_d - 2\chi_e = 0$	x	x	o
$(H_u H_d)^\dagger$	−	−	−	x	x	x
$(H_u H_e)^\dagger$	−	−	−	−	x	x
$(H_d H_e^\dagger)^\dagger$	−	−	−	−	−	x

DFSZ models given in the beginning of this section. One could also see this as a kind of selection criterion.

III. ANOMALY RATIO DISTRIBUTIONS

A. Approach

In the previous section, we reviewed how, for the DFSZ-type axions, the calculation of the anomaly ratio reduces to fixing a $V_{\rm eb}$ and solving the resulting LSE. Hence, in order to calculate all possible anomaly ratios, one has to do exactly that for all possible $V_{\rm eb}$.

In addition, adding different $V_{\rm eb}$ that give rise to the same set of PQ charges, we count how many different sets of charges lead to the same anomaly ratio. This notion of *multiplicity* of each anomaly ratio allows us to allocate a certain probability to each anomaly ratio within the given set of models. We then use this to define lower $|\mathcal{C}_{a\gamma}|$ bounds, above which, most of the probability mass of DFSZ-type axion models can be found.

In the form of a cooking recipe, our procedure can be summarized by the following steps:

(1) Specify the Yukawa sector for a fixed n_D by coupling one doublet to each right-handed fermion. This exhausts the maximal freedom regarding the anomaly ratio.

(2) Write down all possible $V_{\rm eb}$ with $n_D - 1$ terms.

(3) Solve all associated LSEs to find all possible sets of PQ charges. Underdetermined systems are discarded.

(4) Add the potentials of all equal PQ charges to get the most general potential associated with a particular solution. This defines one model for the sake of counting the multiplicity.

(5) For each model, complete the Yukawa sector by adding all Yukawa terms compatible with the PQ and hypercharges.

(6) For each model, calculate the anomaly ratio and count its multiplicity.

We calculate the PQ charges and anomaly ratios numerically using the programming language "Julia" [41]. The "StaticArrays" package [42] allows us to compute the extremely large number of LSEs very fast without heap memory allocation. Since it is not relevant to the acquired solutions, we skip step 5 in practice.

B. Example: $n_D = 3$

Let us demonstrate our approach in the example of DFSZ$_3$ with the Weinberg-Glashow-Paschos condition imposed, i.e., with one Higgs doublet per type of fermion. In this example, there are three possible bilinears, namely $(H_u H_d)$, $(H_u H_e)$, and $(H_d H_e^\dagger)$, together with their complex conjugates. Each bilinear can either be coupled to the singlet, which results in six different terms of the form $HHSS$, or to another bilinear, which results in 36 different quadrilinears of the form $HHHH$. For the latter case, removing terms that are related by Hermitian conjugation and terms that result in no condition reduces the number to nine (see Table I). For $n_D = 3$, the breaking potential consists of either one $HHSS$ and one $HHHH$ term or two $HHSS$ terms. For the former, there are *a priori* 54 possibilities and for the latter, 15, totaling to 69 possibilities for $V_{\rm eb}$ (see Table II).

The resulting 3×3 LSEs consist of the orthogonality relation, $\chi_u v_u^2 - \chi_d v_d^2 - \chi_e v_e^2 = 0$, and the two conditions coming from the potential. Solving the LSEs yields the PQ charges in terms of χ_S, which is then fixed by the well definiteness of the DW number. We can do the following two simplifications for the purpose of calculating the anomaly ratio. First, we can set all VEVs equal to one because E and N are independent of them, and secondly, we can leave χ_S unfixed because it cancels in the anomaly ratio after expressing all PQ charges in terms of χ_S.

Of the 69 minimal potentials found, many have no or degenerate solutions. For example, potentials including a bilinear and its Hermitian conjugate at the same time do not have a solution, and the nine quadrilinears only give six unique conditions for PQ charges. A summary of all solutions can be found in Table II (top). In total, this leaves only 16 different solutions for the doublet charges, for each of which, we have to add all the terms to the potential that give rise to this set of PQ charges.

TABLE II. All possible solutions for PQ charges of Higgs doublets in terms of χ_S (*top*) and anomaly ratios (*bottom*) for the $n_D = 3$ Yukawa sector under consideration. The potential should not produce the same condition twice ("x"), nor does the order of the conditions matter ("−"). "o" denotes combinations of conditions that do not have a solution. Infinite solutions arise when $N = 0$.

$[\chi_u, \chi_d, \chi_e]$	$\chi_u + \chi_d = 2\chi_S$	$\chi_u + \chi_e = 2\chi_S$	$\chi_d - \chi_e = 2\chi_S$	$-\chi_u - \chi_d = 2\chi_S$	$-\chi_u - \chi_e = 2\chi_S$	$-\chi_d + \chi_e = 2\chi_S$
$\chi_u + \chi_d = 2\chi_S$	x	−	−	−	−	−
$\chi_u + \chi_e = 2\chi_S$	$[4/3, 2/3, 2/3]$	x	−	$[0, -2, 2]$	−	−
$\chi_d - \chi_e = 2\chi_S$	$[2/3, 4/3, -2/3]$	$[2, 2, 0]$	x	$[-2, 0, -2]$	$[-2/3, 2/3, -4/3]$	−
$-\chi_u - \chi_d = 2\chi_S$	o	−	−	x	−	−
$-\chi_u - \chi_e = 2\chi_S$	$[0, 2, -2]$	o	−	$[-4/3, -2/3, -2/3]$	x	−
$-\chi_d + \chi_e = 2\chi_S$	$[2, 0, 2]$	$[2/3, -2/3, 4/3]$	o	$[-2/3, -4/3, 2/3]$	$[-2, -2, 0]$	x
$2\chi_u + 2\chi_d = 0$	o	$[2/3, -2/3, 4/3]$	$[-2/3, 2/3, -4/3]$	o	$[-2/3, 2/3, -4/3]$	$[2/3, -2/3, 4/3]$
$\chi_u + \chi_d = 0$	o	$[2/3, -2/3, 4/3]$	$[-2/3, 2/3, -4/3]$	o	$[-2/3, 2/3, -4/3]$	$[2/3, -2/3, 4/3]$
$2\chi_u + 2\chi_e = 0$	$[2/3, 4/3, -2/3]$	o	$[2/3, 4/3, -2/3]$	$[-2/3, -4/3, 2/3]$	o	$[-2/3, -4/3, 2/3]$
$\chi_u + \chi_e = 0$	$[2/3, 4/3, -2/3]$	o	$[2/3, 4/3, -2/3]$	$[-2/3, -4/3, 2/3]$	o	$[-2/3, -4/3, 2/3]$
$2\chi_d - 2\chi_e = 0$	$[4/3, 2/3, 2/3]$	$[4/3, 2/3, 2/3]$	o	$[-4/3, -2/3, -2/3]$	$[-4/3, -2/3, -2/3]$	o
$\chi_d - \chi_e = 0$	$[4/3, 2/3, 2/3]$	$[4/3, 2/3, 2/3]$	o	$[-4/3, -2/3, -2/3]$	$[-4/3, -2/3, -2/3]$	o
$2\chi_u + \chi_d + \chi_e = 0$	$[0, 2, -2]$	$[0, -2, 2]$	$[0, 1, -1]$	$[0, -2, 2]$	$[0, 2, -2]$	$[0, -1, 1]$
$\chi_u + 2\chi_d - \chi_e = 0$	$[2, 0, 2]$	$[1, 0, 1]$	$[-2, 0, -2]$	$[-2, 0, -2]$	$[-1, 0, -1]$	$[2, 0, 2]$
$\chi_u - \chi_d + 2\chi_e = 0$	$[1, 1, 0]$	$[2, 2, 0]$	$[2, 2, 0]$	$[-1, -1, 0]$	$[-2, -2, 0]$	$[-2, -2, 0]$
E/N	$\chi_u + \chi_d = 2\chi_S$	$\chi_u + \chi_e = 2\chi_S$	$\chi_d - \chi_e = 2\chi_S$	$-\chi_u - \chi_d = 2\chi_S$	$-\chi_u - \chi_e = 2\chi_S$	$-\chi_d + \chi_e = 2\chi_S$
$\chi_u + \chi_d = 2\chi_S$	x	−	−	−	−	−
$\chi_u + \chi_e = 2\chi_S$	$8/3$	x	−	$-4/3$	−	−
$\chi_d - \chi_e = 2\chi_S$	$2/3$	$5/3$	x	$14/3$	∞	−
$-\chi_u - \chi_d = 2\chi_S$	o	−	−	x	−	−
$-\chi_u - \chi_e = 2\chi_S$	$-4/3$	o	−	$8/3$	x	−
$-\chi_d + \chi_e = 2\chi_S$	$14/3$	∞	o	$2/3$	$5/3$	x
$2\chi_u + 2\chi_d = 0$	o	∞	∞	o	∞	∞
$\chi_u + \chi_d = 0$	o	∞	∞	o	∞	∞
$2\chi_u + 2\chi_e = 0$	$2/3$	o	$2/3$	$2/3$	o	$2/3$
$\chi_u + \chi_e = 0$	$2/3$	o	$2/3$	$2/3$	o	$2/3$
$2\chi_d - 2\chi_e = 0$	$8/3$	$8/3$	o	$8/3$	$8/3$	o
$\chi_d - \chi_e = 0$	$8/3$	$8/3$	o	$8/3$	$8/3$	o
$2\chi_u + \chi_d + \chi_e = 0$	$-4/3$	$-4/3$	$-4/3$	$-4/3$	$-4/3$	$-4/3$
$\chi_u + 2\chi_d - \chi_e = 0$	$14/3$	$14/3$	$14/3$	$14/3$	$14/3$	$14/3$
$\chi_u - \chi_d + 2\chi_e = 0$	$5/3$	$5/3$	$5/3$	$5/3$	$5/3$	$5/3$

The Yukawa sector in this example does not need any completion since it is already fixed by the Weinberg-Glashow-Paschos condition. Hence, it merely remains to plug into Eq. (13) the different sets of PQ charges, which yields the following possible anomaly ratios (see Table II, bottom),

$$\text{DFSZ}_3\colon \quad \frac{E}{N} = -\frac{4}{3}, \frac{2}{3}, \frac{5}{3}, \frac{8}{3}, \frac{14}{3}. \qquad (21)$$

Counting the multiplicity, we find that 2/3 and 8/3 each appear 2 times with four terms in the potential each, and $-4/3$, 5/3 as well as 14/3 each appear 4 times with three or two terms in the potential each. A visualization of this result, together with all other n_D values, can be found in Fig. 3. For a summary of important statistics, see Table III.

It turns out useful in the following to introduce a compact notation that encodes which doublet couples to which of the nine fermions. For this, we assign to the nine fermions a position in a nine-dimensional row vector with square brackets,

$$
\begin{array}{ccccccccc}
u & c & t & d & s & b & e & \mu & \tau \\
u_1 & u_2 & u_3 & d_1 & d_2 & d_3 & e_1 & e_2 & e_3 \\
[\cdot, & \cdot, & \cdot, & \cdot, & \cdot, & \cdot, & \cdot, & \cdot, & \cdot],
\end{array} \qquad (22)
$$

and write the subscript of the doublets that couple to a certain fermion to the corresponding position. If one doublet couples to multiple fermions, we use the first subscript in the order presented above. For more comprehensive notation, we use fermion type (up-, down-, or lepton-type, short u, d, or e) and generation (1 to 3). For DFSZ$_9$, this row vector would be $[u1, u2, u3, d1, d2, d3, e1, e2, e3]$, while for the original DFSZ$_2$-I model, it would be $[u1, u1, u1, d1, d1, d1, d1, d1, d1]$.

C. Choices for a statistical interpretation

We are considering many different solutions for the Higgs charges. In Sec. III B, we just counted the number of models leading to specific anomaly ratios, but in the end, we want to translate a catalog of models with specific E/N values to a probability distribution of anomaly ratios. To achieve this, we require relative probabilities of the solutions, which are subject to some sort of theoretical prior belief. This belief manifests itself in multiple decisions about:

(i) *The concept of multiplicity* as outlined in Sec. II C.

(ii) *The relative probability of different Yukawa sectors given a specific n_D.*

   A reasonable choice is to demand all solutions with a given n_D to be equally probable. The same applies to different Yukawa sectors. Unfortunately, both cannot be true at the same time because different Yukawa sectors can lead to different amounts of possible solutions. We take the approach of requiring solutions to be equal (given equal multiplicity and same n_D). This also implies not applying any "beauty" arguments for Yukawa sectors, e.g., in favor of coupling patterns that are equal for different fermion types.

(iii) *The relative probabilities of different n_D.*

   For our total anomaly ratio distribution, we treat the probability of all n_D values $2 \leq n_D \leq 9$ as equal. This implies at the same time that we consider any single solution for, e.g., DFSZ$_3$ (of which there are 16), much more probable than any single solution for, e.g., DFSZ$_5$ (of which there are 9.7×10^4). One could also consider it reasonable to additionally penalize models with higher n_D, enhance the probability of models satisfying symmetry arguments (DFSZ$_3$, one Higgs doublet per fermion-type or DFSZ$_9$, one Higgs per right-handed fermion), or consider all charge solutions equally probable. In the latter case, the final histogram would most probably be completely dominated by DFSZ$_9$ due to the much larger amount of unique solutions.

The arguments above all imply a probabilistic approach to model selection, i.e., nature "selects" one of the possible realizations at random. This notion itself may be subject to critique, but in absence of any decisive underlying physical argument singling out any specific model, we deem it to be satisfactory. In Sec. II D, we outline theoretical arguments that might challenge this view.

Even under the assumption of probabilistic model selection, we acknowledge that any of these choices is to some extent a matter of taste. For this reason, it is important to us to provide the raw catalogs and generating code as a supplement to this paper, so the reader is not dependent on our choice.

D. Results for $n_D = 4$–7

Having presented our assumptions leading to a statistical treatment explicitly, we can now proceed to higher numbers of Higgs doublets, for which we investigate multiple different Yukawa sectors. First, we stick to DFSZ$_4$ to DFSZ$_7$, because, for these models, we are able to calculate all possible solutions explicitly.

Figure 1 presents an overview over the anomaly ratio distributions for DFSZ$_4$ models grouped by the different Yukawa sectors. Each of the histograms shows all models of the specified coupling with the explicitly symmetry breaking potential V_{eb} consisting of $k \geq 1$ *HHSS-* and $3 - k$ *HHHH*-terms. The result does not depend on fermion generation since the construction of the Higgs charges as well as Eq. (13) treat all generations equally. Yukawa sectors with special coupling to a lepton have histograms symmetric around $5/3$, while the histograms for up- and down-type special couplings are mirrored around $5/3$.

The reason for this is a symmetry in our construction as well as in Eq. (13): For every n_D, since we consider all possible Yukawa sectors as outlined above, every solution has a corresponding one with

$$\chi_{\tilde{u}_i} \to -\chi_{d_i}$$
$$\chi_{\tilde{d}_i} \to -\chi_{u_i}. \tag{23}$$

This is due to up-type and down-type quarks being treated equally in the construction except for the sign of their hypercharges. In the example above, all solutions for the Yukawa sector $[u1, u1, u3, d1, d1, d1, e1, e1, e1]$ have a corresponding solution in the Yukawa sector $[u1, u1, u1, d1, d1, d3, e1, e1, e1]$ under the above mentioned transformation. Solutions that relate via Eq. (23) can easily be seen to have anomaly ratios relating by

$$\frac{\tilde{E}}{N} \to \frac{10}{3} - \frac{E}{N}, \tag{24}$$

which is a mirror symmetry around $\frac{5}{3}$.

If we add up all nine histograms of Fig. 1, i.e., do not treat any Yukawa sector preferentially, we obtain the distribution shown in Fig. 3 (second row, left). Due to the symmetries of the nine contributing Yukawa sectors, the distribution is symmetric around $5/3$ as well. The biggest number of models coincides with the two possible values for the DFSZ$_2$ model: $2/3$ and $8/3$. Both of these statements are true for $n_D \in [4, 7]$, as Fig. 3 shows (second row, third row left).

With increasing n_D, we find an increasing number of unique anomaly ratios and more extreme E/N values. Anomaly ratios $E/N = 5/3 + k$ with $k \in \mathbb{Z}$ are highly favored for $n_D \geq 5$ compared to other E/N values,
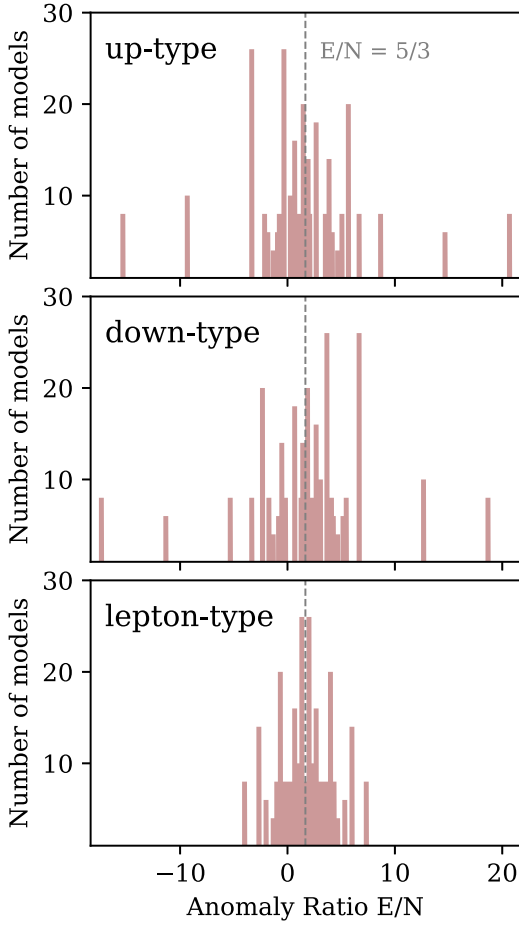
FIG. 1. Anomaly ratio distributions for DFSZ-type models with four Higgs doublets. Two Higgs couple to the fermions specified in the panels with the other two Higgs covering the remaining two fermion types invariant with respect to fermion generation. For example, the Yukawa sectors $[u1, u1, u3, d1, d1, d1, e1, e1, e1]$, $[u1, u2, u1, d1, d1, d1, e1, e1, e1]$, and $[u1, u2, u2, d1, d1, d1, e1, e1, e1]$ are all equivalent and have anomaly ratio distributions as shown in the top panel. Note that the up-type and down-type cases are mirrored around 5/3.
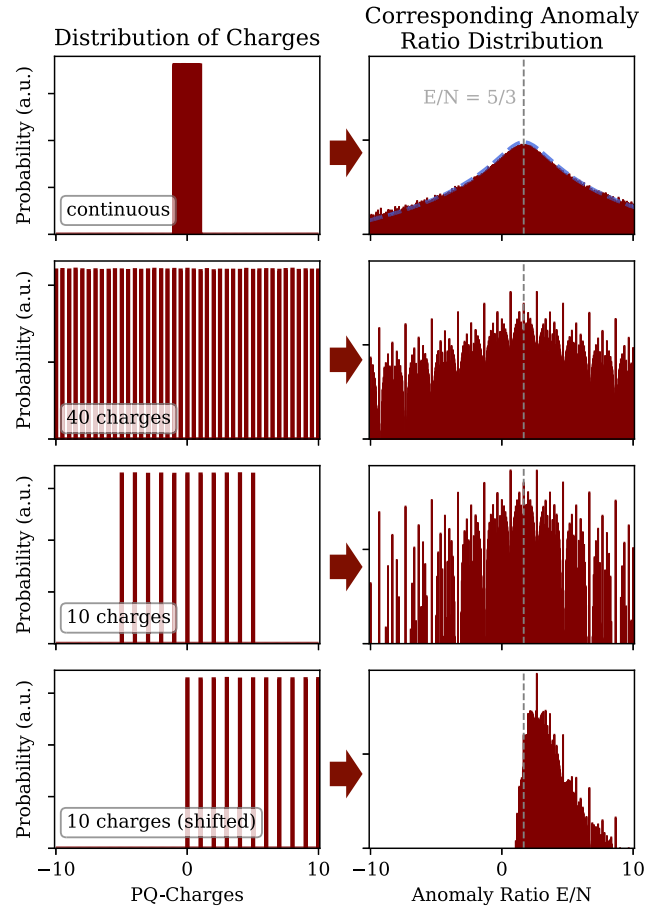
FIG. 2. Influence of drawing charges from different distributions on the resulting anomaly ratio distribution, using Eq. (13). More unique charges lead to a smoother anomaly ratio distribution, irrespective of their distribution. Charge distributions centered around 0 produce anomaly ratio distributions centered around 5/3. The dashed blue line in the top right panel denotes the fit presented in Eq. (25).

especially for odd k. We see this very characteristic, peaked spectrum evolving: E/N values with high probability tend to have their probabilities shrink with increasing n_D, whereas low probability E/N values behave in the opposite manner. In Fig. 3, one can most easily see this evolution at big anomaly ratios $E/N \gtrsim 10$.

Let us try to understand this trend from a purely mathematical perspective:

$$\frac{E}{N} = \frac{2}{3} + 2 \frac{\sum_i \chi_{u_i} + \chi_{e_i}}{\sum_i \chi_{u_i} + \chi_{d_i}}$$

is a function with nine variables, the values of each of which can be thought of as being drawn from a specific distribution. In Fig. 2, we show the effect of using different distributions for the variables on the outcome of the

function. A continuous, flat charge distribution of arbitrary width produces a smooth, fat-tailed E/N distribution. If the median of the charges is 0, the median of the distribution is at 5/3 (Fig. 2, top three rows). Allowing only positive values for the charges shifts the distribution to higher values, with a median of 8/3 and makes $E/N < 0$ impossible (Fig. 2, bottom row). The fewer distinct input values for the charges are used, the more peaked the anomaly ratio structure becomes; i.e., anomaly ratios with high relative probability see their likelihood increased and vice versa. This also leads to fewer possible unique E/N-values.

The continuum limit with its vanishing skewness and positive kurtosis can be approximated in analytic form via a Pearson type VII distribution [43],

$$p\left(\frac{E}{N}\right) = \frac{1}{\alpha B(m - \frac{1}{2}, \frac{1}{2})} \left[1 + \left(\frac{\frac{E}{N} - \lambda}{\alpha}\right)^2\right]^{-m}, \quad (25)$$
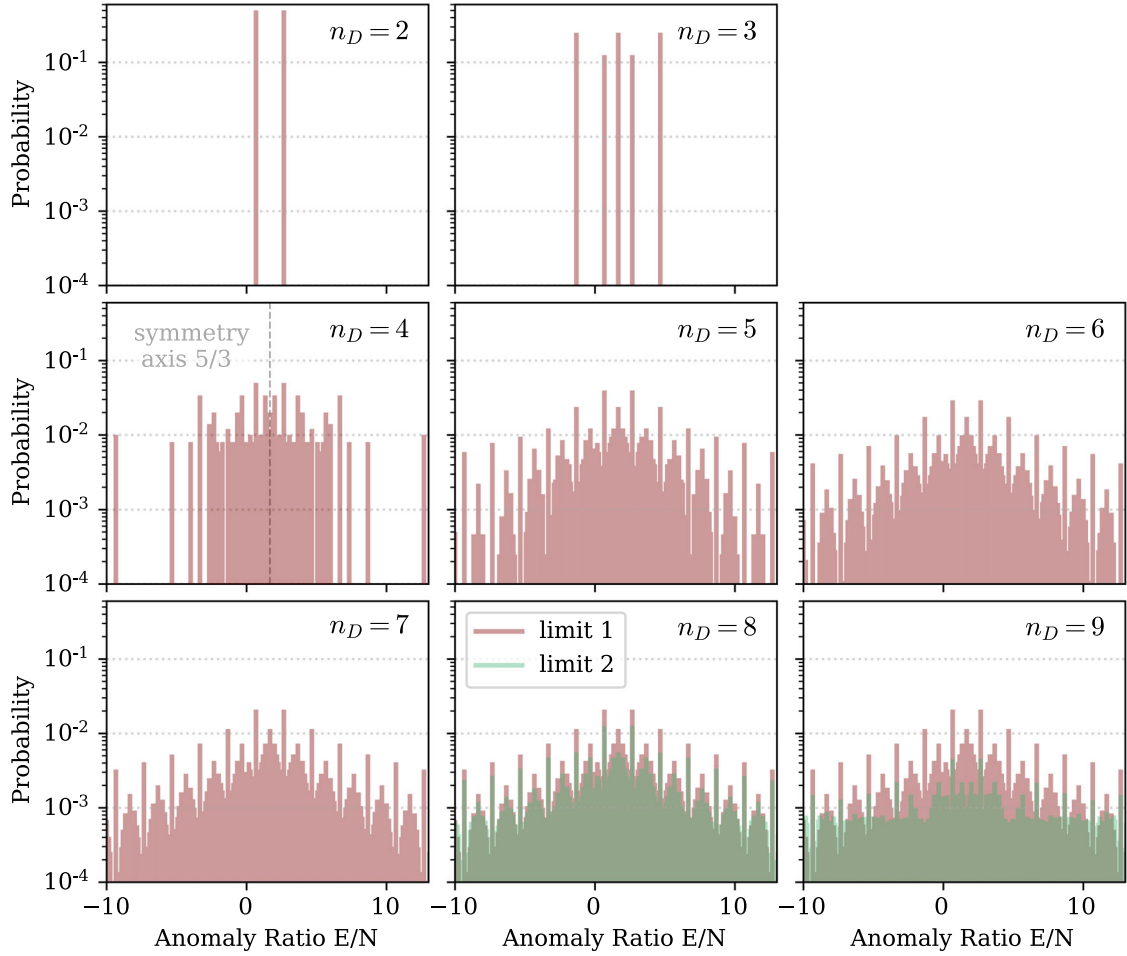
FIG. 3. Anomaly ratio distributions for different numbers of Higgs doublets. All histograms are symmetric around 5/3. $n_D \geq 5$ display a characteristic peaked structure, which becomes smoother with increasing n_D. DFSZ$_8$ and DFSZ$_9$ could not be fully calculated; the two semitransparent colors denote the two estimates as discussed in the text. Note that limit 2 only slightly exceeds limit 1 at big absolute anomaly ratios for $n_D = 8$ as well as $n_D = 9$.

with reasonable fit parameters $\lambda = 5/3$, $\alpha = 7/4$, and $m = 1$, and Beta function B with $B(1/2, 1/2) = \pi$.

Following these insights from a mathematical perspective, it can be understood that the histograms for larger n_D should be smoother, considering that there are more unique solutions (Table III). Note, however, that this effect neglects the influence of choosing different probabilities for different solutions. Nonuniform probabilities reduce the effective number of different solutions.[1] Using our approach of adding all possible potential terms for one solution of charges leads to more comparable probabilities for the charges than if we had separately considered all potentials with the minimal amount of terms to fix the PQ charges (minimal potentials). Therefore, the effect of nonuniform

charge probabilities is clearly subdominant for DFSZ$_5$ to DFSZ$_7$. We expect this to still be the case even for DFSZ$_8$ and DFSZ$_9$.

E. Extrapolation to $n_D > 7$

While our procedure, in principle, works for any number of doublets, for larger n_D, it requires solving an extremely large number of LSEs. In order to see how many, let us estimate the number of all possible terms for step 2 with an arbitrary n_D. Since the number of possible bilinears is $n_B = \binom{n_D}{2}$ plus their Hermitian conjugate, there are $2n_B$ terms of the form $HHSS$. Regarding the quadrilinears, this results in $(2n_B)^2$ possible terms. Written as a matrix, this yields

$$
\begin{array}{c}
\\
HH \\
(HH)^{\dagger}
\end{array}
\begin{array}{cc}
HH & (HH)^{\dagger} \\
\begin{pmatrix} A & B \\ C & D \end{pmatrix}, &
\end{array}
\tag{26}
$$

---

[1]Just think of the extreme case of say, a charge distribution with 100 unique solutions, in which 10 solutions are 1000× more probable than the other 90. The resulting E/N distribution will behave more as if it came only from 10 unique charges than as if it had 100.

TABLE III.   Important statistics of DFSZ-type models broken down by number of Higgs doublets n_D. We include information on the model with maximal photon coupling $\widehat{E/N}$ from Eq. (29) and the percentage of models that have minimal photon coupling (photophobic, $|E/N - 1.92| < 0.04$). "x" denotes values that could not be estimated.

n_D	#V_{eb}	Unique solutions	Unique E/Ns	$\widehat{E/N}$	% Photophobic	% $N_{\mathrm{DW}} = 1$
2	2	2	2	2/3	0	0
3	54	16	5	−4/3	0	0
4	52614	996	83	−52/3	1.4	6.00
5	6.65×10^7	9.7×10^4	432	−112/3	1.52	6.64
6^a	$\lesssim 4 \times 10^9$	$> 2.19 \times 10^6$	1680	−238/3	1.37	5.83
7^a	$\lesssim 7 \times 10^{12}$	x	6256	−466/3	1.39	5.19
8^b	$\lesssim 2 \times 10^{16}$	x	> 11617	$< -628/3$	x	x
9^b	$\lesssim 1 \times 10^{20}$	x	$\gg 14122$	$< -1216/3$	x	x

^{a}For $n_D \geq 6$, number of potentials V_{eb} and "unique solutions" are estimates. Number of minimal potentials calculated via Eq. (27), many of which will be unphysical and not produce valid solutions for PQ charges. The "unique solutions" column gives the number of solution found in sample, for which data exists.

^{b}For $n_D \geq 8$, we did not calculate all possible models; therefore, we have no exact value neither for the number of unique E/N, nor for the percentage of photophobic models or models with $N_{\mathrm{DW}} = 1$. $\widehat{E/N}$ was estimated as shown in Sec. III F.

where A denotes the submatrix formed by all terms of the form $HHHH$, B by $HH(HH)^{\dagger}$, and so on. However, as in the DFSZ$_3$ example, there are several equal terms in this matrix that should not be counted. First of all, the whole matrix is symmetric. Secondly, since Hermitian conjugated terms are equal, D is completely redundant with respect to A. Lastly, B is antisymmetric so that the number reduces to n_B^2 quadrilinears.

From the set of all terms, we need to pick $n_D - 1$ terms where at least one must be of the form $HHSS$. Hence, we can pick between 1 and $n_D - 1$ terms of the form $HHSS$, then fill up with $HHHH$ terms, and repeat this for all possible amounts of $HHSS$ terms (ignoring equivalences in the case of multiple $HHSS$ terms). The total number of possible V_{eb} can then be estimated by

$$N_{\mathrm{tot}}(n_D) \sim \sum_{j=0}^{n_D-2} \binom{2n_B}{1+j} \binom{n_B^2}{n_D - 2 - j}, \quad (27)$$

which, at the same time, is the number of LSEs that needs to be solved.

In principle, we can again perform the simplifications used for the DFSZ$_3$ example, namely setting all VEVs to one and not fixing χ_S, but regardless of these simplifications, the computation time rises exponentially with n_D. While $N_{\mathrm{tot}}(n_D = 3) = 69$ is easily manageable, for, e.g., $n_D = 8$, the number of possibilities becomes $N_{\mathrm{tot}}(n_D = 8) \approx 2 \times 10^{16}$. Thus, computing requirements for solving all LSEs beyond DFSZ$_7$ are prohibitive.

An easy solution to the computationally prohibitive number of LSEs would be to sample the (minimal) potentials. However, due to step 4 in our approach, this is not possible without introducing a bias: A multitude of minimal potentials can lead to the same solution. In our approach, all of them belong to the same model, which,

for this reason, has a very long potential and is likely to be found by any sampling algorithm. On the opposite side, there are also models that can just be found with one or two minimal potentials. Sampling in the space of minimal potentials therefore leads to biased sampling in the space of models.

An alternative estimation for the DFSZ$_8$ and DFSZ$_9$ distributions can come from the following considerations. If a large enough number of theories is considered, Fig. 2 (top, right) and Fig. 2 (third row, right) can be viewed as extremal cases for the anomaly ratio distribution. "Extremal" in this context should not be understood in terms of an upper or lower limit on individual E/N bins; after all, we are considering (normalized) probability measures. Rather, Fig. 2 (top row, right) is very smooth, whereas Fig. 2 (third row, right) is very peaked. Before applying it, let us quantify this criterion by looking at the cumulative sum of anomaly ratios below a specific value. Similarly to the two sample Kolmogorov-Smirnov-test, we define smoothness of an anomaly ratio distribution $f(E/N)$ as

$$\max_x \left| \sum_{E/N < x} f(E/N) - \sum_{E/N < x} c(E/N) \right|, \quad (28)$$

where $c(E/N)$ represents the continuous distribution as shown in Fig. 2 (top, right). Equation (28) defines the maximum of the difference for all anomaly ratios in the cumulative sum of the distribution compared to the case of continuous charges as a possible metric for this task. In Sec. IV A, we will see the close connection of this metric to the relevant observable. The metric runs from one to zero (by construction for the continuous distribution). For DFSZ$_3$, the value is 17%, for DFSZ$_4$ already 5.7%, and down to 1.4% for DFSZ$_7$.

We want to be able to roughly constrain the smoothness of the DFSZ$_8$ and DFSZ$_9$ anomaly ratio distributions. From our results for DFSZ$_3$ to DFSZ$_7$, we saw that the higher the number of doublets, the smoother the anomaly ratio distribution becomes. From investigations of the biased sampling for $n_D = 6$ and $n_D = 7$, where the true distributions were available, we see that sampling leads to less smooth distributions. This means that the distribution for $n_D = 8$ or $n_D = 9$ is expected to be smoother than their respective sampled distribution and the $n_D = 7$ distribution. In Fig. 3, we use $n_D = 7$ as one estimate, denoted as "limit 1."

The other estimate, overestimating the smoothness, can come from the observation that the difference in smoothness of the distributions is smaller between DFSZ$_6$ and DFSZ$_7$ than between DFSZ$_5$ and DFSZ$_6$. Extrapolating the histograms beyond $n_D = 7$ using the difference of the distributions of DFSZ$_6$ and DFSZ$_7$ should therefore yield anomaly ratio distributions, which are smoother than our actual expectation. In Fig. 3, we subtract the difference once to reach the estimate for $n_D = 8$ and twice for $n_D = 9$, denoted as "limit 2." For the metric described by Eq. (28), we find 0.73% and 0.71% for DFSZ$_8$ and DFSZ$_9$, respectively.

The approach presented here should not be viewed as presenting hard limits for the anomaly ratio distributions for eight or nine Higgs doublets, but rather a rough estimate. The difference in probability in Fig. 3 looks substantial only due to the logarithmic axis. Both estimates are much closer to the continuous case of Fig. 2 (top, right) than to the peaked one of Fig. 2 (third row, right) in the sense that only very little of their probability mass lies at unique E/N values and rather in a continuum.

F. Constructing extreme $|g_{a\gamma}|$

Another problem that arises by sampling potentials as described in the previous paragraphs is that it is very unlikely to find the anomaly ratio corresponding to the maximum axion-photon coupling, which we denote as

$$\widehat{E/N} = \mathrm{argmax}_{E/N}(|E/N - 1.92|). \qquad (29)$$

This anomaly ratio, however, is very useful for constraining the region of DFSZ-type models. For this reason, we give a procedure on how to construct an estimate for it. Before turning to this procedure though, let us note that due to the symmetry around $E/N = 5/3$, in absence of selection criteria, $\widehat{E/N}$ is not given by the largest possible anomaly ratio but the smallest.

The procedure is based on observations of the LSEs that led to $\widehat{E/N}$ for the smaller numbers of doublets. There, we found that any of the LSEs leading to $\widehat{E/N}$ of DFSZ$_4$ can be extended to an LSE leading to $\widehat{E/N}$ for DFSZ$_5$. The same behavior can be seen from DFSZ$_5$ to DFSZ$_6$ and in a slightly different form from DFSZ$_3$ to DFSZ$_4$. We do not have a rigorous mathematical reason why this is the case, so applying it to larger n_D is more of an educated guess. However, it turns out to give extreme anomaly ratios, so we use it to systematically estimate $\widehat{E/N}$.

The procedure goes as follows. First, we take all LSEs that lead to $\widehat{E/N}$ for a number of doublets where all solutions are known, say $n_D = 6$. Secondly, we add one additional Higgs doublets by specifying the Yukawa sector for the new doublet. Thirdly, we adjust the orthogonality relation appearing in all LSEs depending on what type of doublet is added. Then, we add one additional relation to the LSEs, solve them, and calculate the anomaly ratio. After that, we repeat this for every possible relation and every possible Yukawa sector. Finally, we extract the LSEs with the smallest anomaly ratio.

This results in highly negative anomaly ratios. However, we found for DFSZ$_9$ that taking the resulting LSEs and systematically exchanging one (or more if the runtime is acceptable) of the relations, new LSEs are found that give even smaller anomaly ratios. In DFSZ$_9$, for instance, the smallest anomaly ratio we construct in this way is $E/N = -1216/3$, and it is generated by the terms,

$$(H_{d_2}^\dagger H_{e_1})(H_{d_2}^\dagger H_{d_1}), \qquad (H_{u_1} H_{d_1})(H_{u_1} H_{d_2}),$$
$$(H_{u_3}^\dagger H_{u_1})(H_{u_3}^\dagger H_{u_2}), \qquad (H_{e_1}^\dagger H_{d_1})(H_{e_1}^\dagger H_{e_2}),$$
$$(H_{e_2}^\dagger H_{d_1})(H_{e_2}^\dagger H_{e_3}), \qquad (H_{u_2} H_{d_3})(H_{u_1}^\dagger H_{u_2}),$$
$$(H_{d_3} H_{u_1})(H_{d_1}^\dagger H_{d_3}), \qquad (H_{d_1} H_{u_1})S^\dagger S^\dagger.$$

G. Comparison with KSVZ-type models

In [20], the authors add all anomaly ratios of phenomenologically allowed KSVZ-type models, irrespective of the number of quarks, allowing one to add or subtract quark representations. This means that a single model with $N_Q = 9$ quarks, of which there are $> 1 \times 10^5$, is deemed equally probable as a single model with $N_Q = 1$, of which there are only 15. The distribution is therefore dominated by $7 \lesssim N_Q \lesssim 21$. If we used a similar approach for our DFSZ-type models, extrapolating the evolution of unique solutions with increasing n_D, the resulting distribution would be indistinguishable from the DFSZ$_9$ case. In Sec. III C, we argued to instead use an approach in which all separate values for n_D are equally probable. Since raw data was provided by [20], we are able to weight their KSVZ data in a way that gives equal probability to all values of N_Q.[2]

Using this weighting, their data can be compared with our DFSZ results on a fair basis, and we show the result in

---

[2]So, now the 15 models with $N_Q = 1$ combined are equally likely as all $> 1 \times 10^5$ models with $N_Q = 9$ combined.
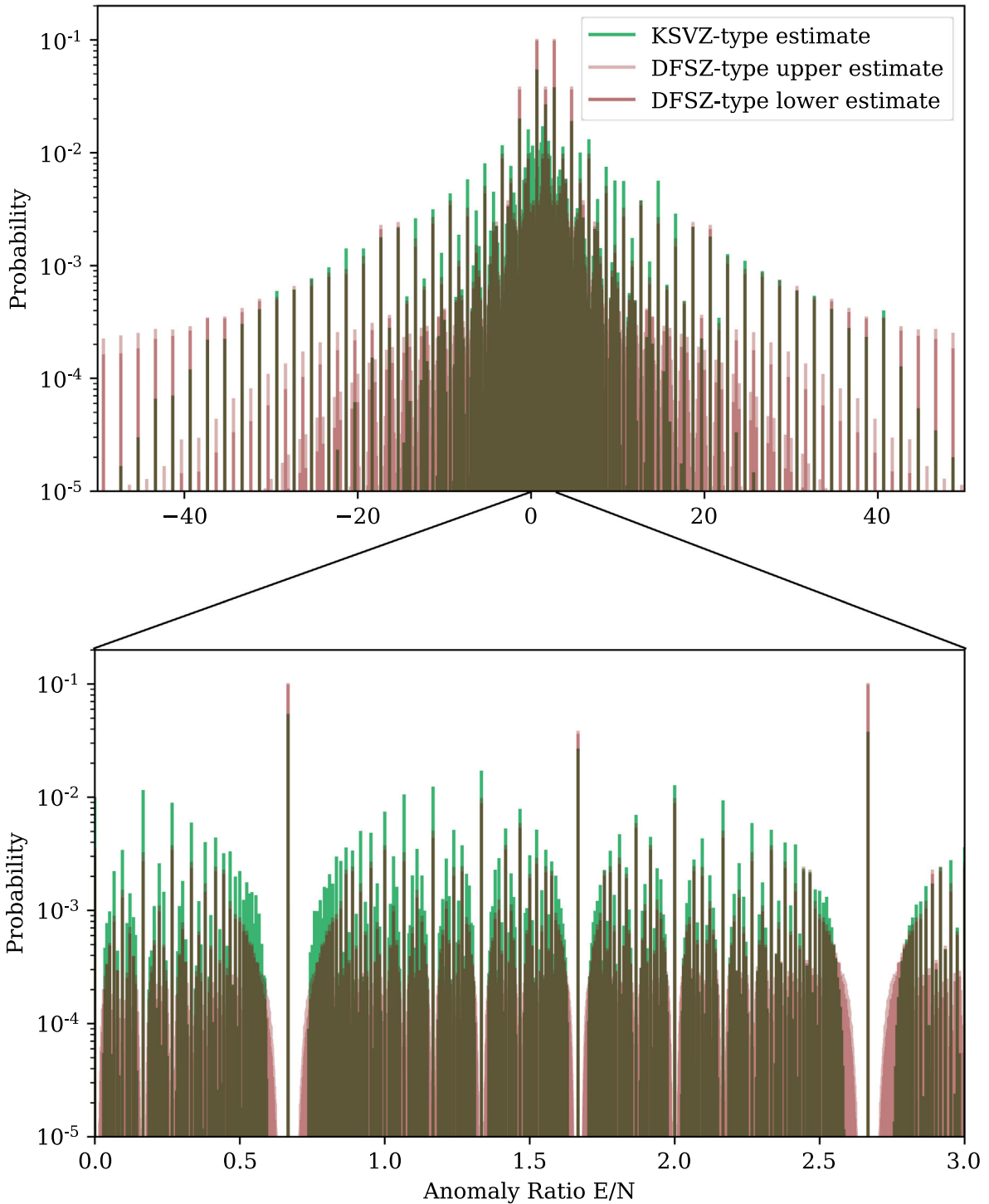
FIG. 4.   Comparison between anomaly ratio distributions for KSVZ-type and DFSZ-type axion models. The KSVZ-type estimate of [20] includes all phenomenologically allowed models, adding and subtracting quark representations, and assumes every model to be equally likely. Our DFSZ-type results include calculations for $DFSZ_2$ to $DFSZ_7$ and estimates for $DFSZ_8$ and $DFSZ_9$, giving equal probability to each n_D. For DFSZ-type, the different shades denote maximum and minimum for each bin under the two limits for $DFSZ_8$ and $DFSZ_9$ described above.

Fig. 4. Nevertheless differences remain: The authors of [20] were able to apply strict selection criteria, significantly reducing the number of viable models. We did not find similar stringent selection criteria, so our catalog reflects the full set of models rather than a preferred set. A comparison between the two types of models or a combined axion band should therefore not be seen as final, but only as incorporating all selection criteria known so far.

Also note that in our case, a model with higher n_D is always less likely than a model with lower n_D, which can be seen as an appropriate penalty for introducing more degrees of freedom to the model. In our weighting scheme for KSVZ data from [20], this is not the case, since for, e.g., $N_Q = 28$, they find only 510 preferred models, much less than for $N_Q = 9$, making a single model with $N_Q = 28$ more likely than a single model with $N_Q = 9$ in our approach.

One can clearly see the effect of the equal weights for all n_D in Fig. 4 in the region around $E/N = 5/3$: The five E/N values of the DFSZ$_2$ and DFSZ$_3$ models show highly elevated probability due to their big relative probabilities (compare Fig. 3). The effect of the two estimates for DFSZ$_8$ and DFSZ$_9$ only becomes substantial at low absolute probabilities and above $|E/N| \gtrsim 20$. We find the KSVZ results to also form a peaked structure similar to the DFSZ case, which only becomes visible in a very finely binned histogram. In fact, for E/N values excluding DFSZ$_2$ and DFSZ$_3$, the DFSZ-type histograms are less peaked than the KSVZ-type ones, with decreased probability at moderately big $|E/N|$ and significantly increased probability for $|E/N| \gtrsim 40$. This trend does not translate to the biggest possible axion-photon coupling, however. We find a maximal $|g_{a\gamma}|$ at $\widehat{E/N} > -1216/3$, which is comparable to the KSVZ case for $N_Q \leq 9$ before any phenomenological constraints ($\widehat{E/N} = -1312/3$).

Concerning models with smallest axion to photon couplings, in the following, photophobic models are defined the same way as in [20] by their anomaly ratio E/N being compatible with with vanishing $g_{a\gamma}$ within one sigma theoretical uncertainty [see Eq. (2)]. Table III shows that there is no clear trend toward a higher or lower percentage of photophobic models with increasing n_D. As discussed in Sec. III D, the anomaly ratio distribution becomes smoother with increasing n_D: Peaks become less pronounced and anomaly ratios with low probability become more likely. The absence of a clear trend hints at the photophobic region being right in the middle between those two extremes. Overall, the percentage of photophobic models we find for DFSZ-type models with $n_D \leq 7$ is similar to the KSVZ case.

In both, KSVZ and DFSZ type of model probability distributions, the probability close to the highest peaks is strongly suppressed (Fig. 4, bottom). The effect is less severe for DFSZ-type than for KSVZ-type ones because as noted before, the former are less peaked if we subtract the effect of DFSZ$_2$ and DFSZ$_3$.

Upon closer inspection, the distribution of KSVZ-type models is not symmetric around $5/3$ however, unlike the DFSZ-type one. Median and mean anomaly ratios are $E/N|_{\text{mean}} = 1.43$ and $E/N|_{\text{median}} = 1.30$, respectively, whereas for DFSZ-type models both are exactly $E/N|_{\text{mean}} = E/N|_{\text{median}} = 5/3$. These values remain unchanged, even if only considering the subset of $N_{\text{DW}} = 1$ models. The

deviation from $5/3$ in the KSVZ-type models of [20] may arise due to the phenomenological selection criteria they impose.

IV. IMPLICATIONS FOR AXION SEARCHES

A. $C_{a\gamma}$ Cumulative distribution function

We have so far derived probability mass functions for the anomaly ratio from theoretical assumptions for different DFSZ-type theories. To be able to understand the implications for axion searches, we need to map these E/N distributions into $g_{a\gamma}$ space via Eq. (2). In order to be independent of the axion mass, we plot our results with respect to the unitless quantity $|C_{a\gamma}|$ defined in Eq. (2).

Traditionally two-sided axion bands centered around the region of maximal probability are given in this case [19,20,44–46]. However, usually an experiment is sensitive to all axion-photon couplings above a certain threshold $|C_{a\gamma}|^{\text{min}}$. We therefore deem it to be also relevant for experiments to post a one-sided limit that has to be reached in order to be sensitive to, e.g., 68% of all DFSZ-type models given a specific axion mass. For this purpose, we use a cumulative distribution function (CDF) plotted against $|C_{a\gamma}|$, which can be understood as the combined theoretical prior probability of models with $|C_{a\gamma}|(\text{model}) > |C_{a\gamma}|^{\text{min}}$.

Since we are treating the anomaly ratio as a random variable coming from a distribution that we try to determine, we have to treat the second part of $C_{a\gamma}$, the next-to-leading order QCD corrections $C_{a\gamma\gamma}^{(0)}$, in the same way. We model its uncertainty as a normal distribution $\mathcal{N}(1.92, 0.04)$ with mean 1.92 and standard deviation 0.04. This smooths out steps in the CDF from high probability E/N values, especially for anomaly ratios close to the mean value of $C_{a\gamma\gamma}^{(0)}$.

B. Experimental constraints

Under the assumptions outlined above, we note that the anomaly ratios of the DFSZ$_2$ and DFSZ$_3$ models still are the most notable features in the probability distribution, even for all possible DFSZ models. However, since only one value of the anomaly ratio is realized in nature, reaching sensitivity to these models may be either not necessary or not sufficient.

Figure 5 shows the resulting theoretical prior probability of DFSZ-type axion models with $|C_{a\gamma}|$ higher than a specific value. We break the results down by possible values of n_D. Let us first discuss the "all N_{DW}"-case, in which the domain wall number does not present a meaningful selection criterion. DFSZ$_3$ models have zero probability above $\log |C_{a\gamma}| \gtrsim 0.5$. Should an axion be found above this value that can be determined to be of DFSZ-type, this would imply the existence of $n_D > 3$ Higgs doublets. The impact of the prominent peaks of maximal probability between $E/N = -4/3$ or $E/N = 14/3$ on the
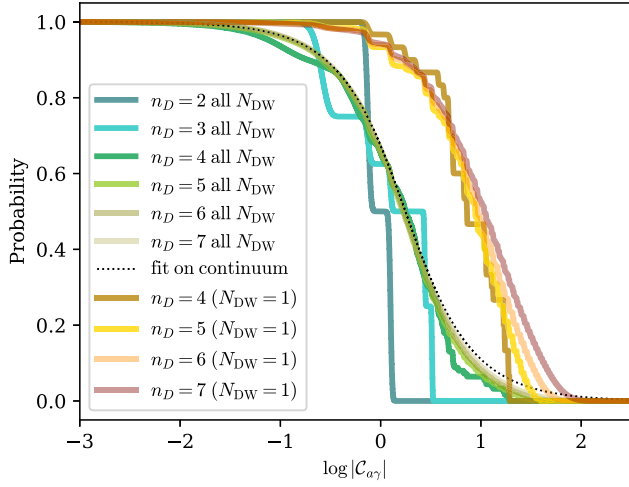
FIG. 5. Cumulative probability of models with $|\mathcal{C}_{a\gamma}|$ higher than the indicated values. The plot includes DFSZ-type models of arbitrary domain wall number N_{DW} with DFSZ_3 to DFSZ_7 as well as $N_{\mathrm{DW}} = 1$ models for DFSZ_4 to DFSZ_7 (for smaller n_D, no $N_{\mathrm{DW}} = 1$ models exist). The CDFs become smoother with increasing n_D, with DFSZ_6 and DFSZ_7 already being almost indistinguishable. $N_{\mathrm{DW}} = 1$ models have systematically larger $|\mathcal{C}_{a\gamma}|$, shifted by almost one order of magnitude. The dashed line indicates the analytic fit on the continuum limit from Eq. (30).

cumulative probability is only minor for theories with $n_D \geq 5$. Since the CDFs for DFSZ_6 and DFSZ_7 are already almost indistinguishable, we refrain from additionally plotting our estimates for higher n_D. In fact, the relative difference on $|\mathcal{C}_{a\gamma}|$ exclusion limits between our two ways of estimating the smoothness of the DFSZ_8 and DFSZ_9 distributions is below the percent level. For the purpose of $|\mathcal{C}_{a\gamma}|$ exclusion limits, the two estimates are therefore virtually equivalent. In the following, we use limit 2, the extrapolation estimate.

It is possible to obtain a reasonable analytic estimate for the cumulative probability distribution by going back to the analytic anomaly ratio fit from Eq. (25). For $|\mathcal{C}_{a\gamma}|$, it translates to

$$p(|\mathcal{C}_{a\gamma}|)$$

$$= 1 - \frac{\tan^{-1}\left[\frac{4}{7}\left(|\mathcal{C}_{a\gamma}| - \frac{19}{75}\right)\right] + \tan^{-1}\left[\frac{4}{7}\left(|\mathcal{C}_{a\gamma}| + \frac{19}{75}\right)\right]}{\pi},$$

$$(30)$$

which is plotted as a dotted line in Fig. 5.

Now contrast the full set of DFSZ_4 to DFSZ_7 models with the respective subsets having $N_{\mathrm{DW}} = 1$. The latter models could be considered preferred in the postinflationary scenario due to cosmological energy density arguments (see Sec. II D). $N_{\mathrm{DW}} = 1$ models display $|\mathcal{C}_{a\gamma}|$ values almost an order of magnitude higher on average than the full set and are therefore much easier to detect. Similarly to

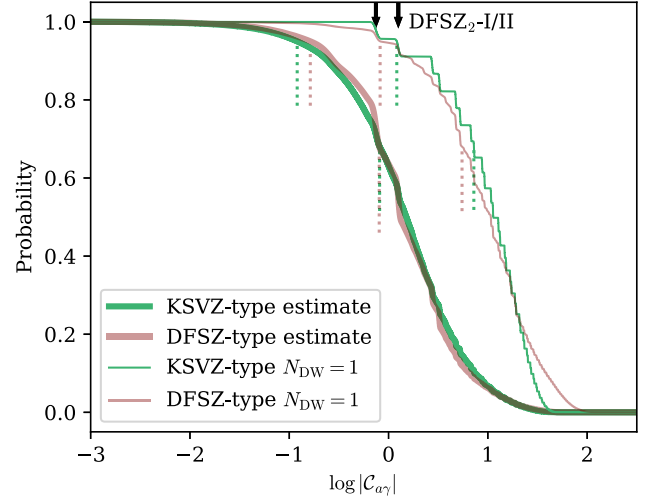FIG. 6. Cumulative probability of models with $|\mathcal{C}_{a\gamma}|$ higher than the indicated values for the complete set of DFSZ-type and KSVZ-type models as well as for models with $N_{\mathrm{DW}} = 1$ specifically (thin lines). One sided 95% and 68% limits for both cases are given with colored vertical dotted lines. The arrows at the top indicate the location of DFSZ_2-I and DFSZ_2-II.

the "all N_{DW}"-case, higher n_D values tend to have smoother distributions. It therefore seems reasonable to analogously introduce our two estimates where the difference with respect to the $|\mathcal{C}_{a\gamma}|$ limits between the two estimates is again below the percent level. We again use limit 2, the extrapolation estimate, in the following.

We show Fig. 6 for a comparison of the CDFs for DFSZ- and KSVZ-type models. In general, both types are very similar for all $|\mathcal{C}_{a\gamma}|$. Only for DFSZ-type models with
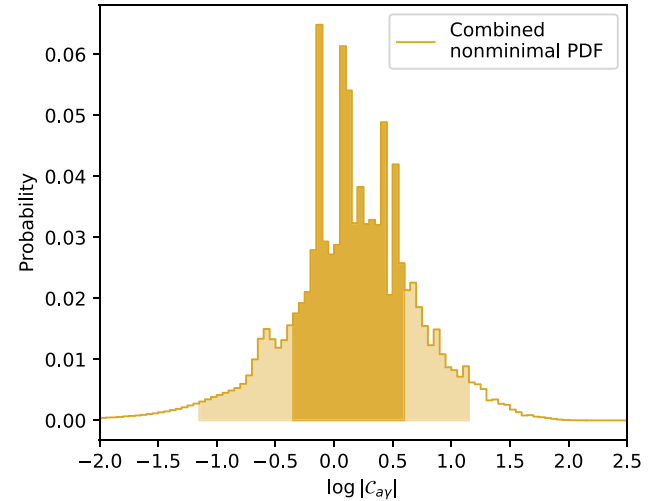

FIG. 7. Probability density in $\log|\mathcal{C}_{a\gamma}|$-space of the combined DFSZ-type and KSVZ-type "all N_{DW}"-case. Central 68% and 95% regions used for Fig. 8 are indicated in different shades of yellow. Note that the underlying distribution is discrete, and any illustration will, in part, depend on the binning chosen.
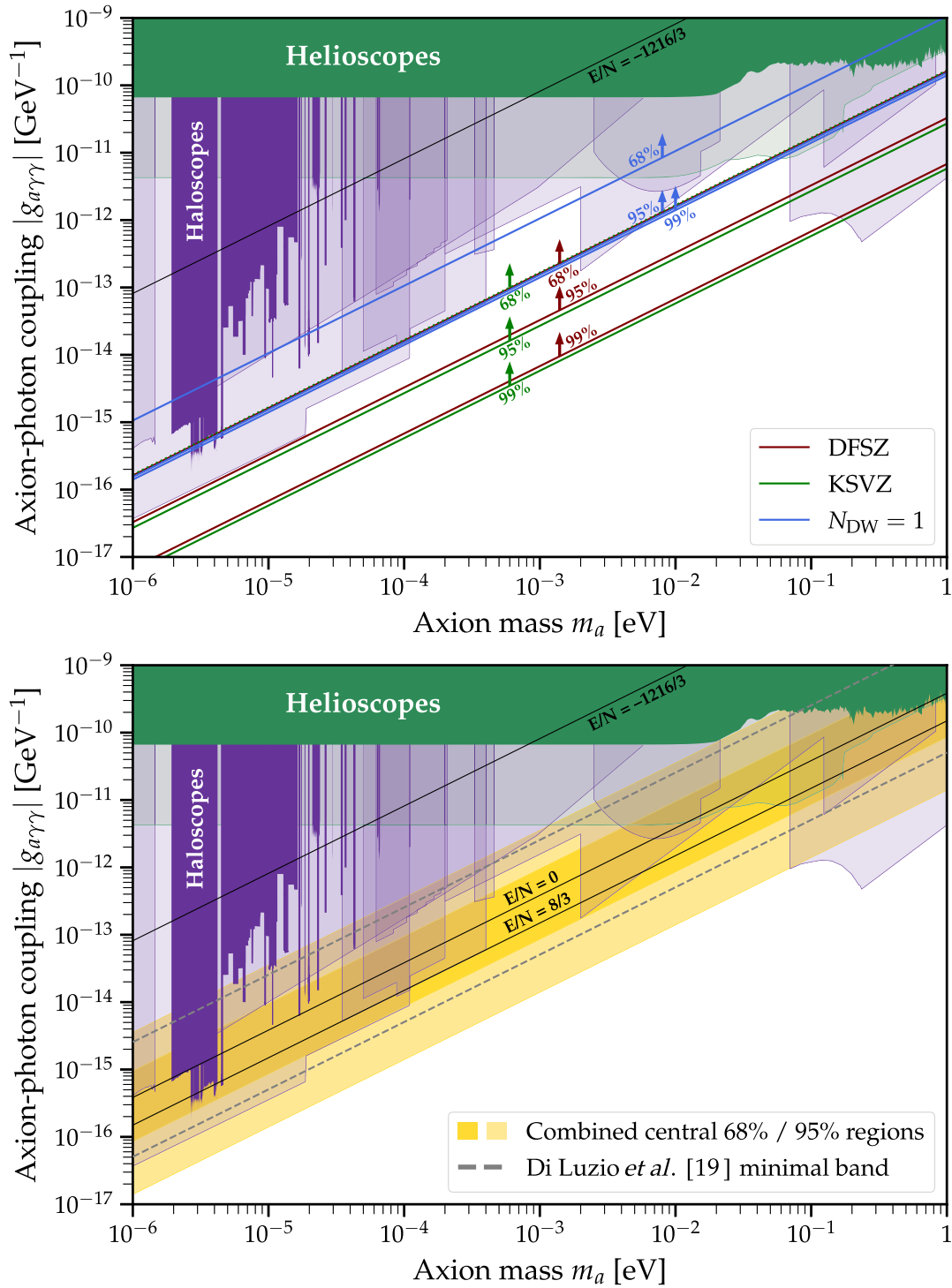
FIG. 8. Top: 68%, 95%, and 99% limits for the complete preferred KSVZ case [20], our complete DFSZ case (using extrapolation for DFSZ$_8$ and DFSZ$_9$) as well as the combined $N_{\mathrm{DW}} = 1$ case. The highest DFSZ-type coupling found is shown in black ($E/N = -1216/3$). DFSZ$_2$-I and DFSZ$_2$-II roughly coincide with the 68% limit of the complete DFSZ case and the 95% limit of the $N_{\mathrm{DW}} = 1$ case, respectively. Bottom: Central 68% and 95% regions for the case combining all preferred KSVZ and all DFSZ models together with a previous band from Di Luzio *et al.* [19] for comparison. We show helioscope limits and forecasts [47–49] in green as well as limits and forecasts from various haloscope experiments [50–93] in purple. For reference, we also show the $E/N = 0$ and $E/N = 8/3$ lines in black. All experimental limits shown here are Frequentist in nature and should therefore only be seen as a rough comparison with respect to our Bayesian prior results. For the full cumulative probability from which the three limits shown in the top panel are taken, see Fig. 6, and for the combined probability density from which the band in the bottom panel is derived, see Fig. 7. (Plotted with tools by O'Hare [94].)

TABLE IV. $|\mathcal{C}_{a\gamma}|$ lower prior limits for selected combinations of models. All limits shown are one sided, so a central 68% band can be constructed with values given for 16% and 84% and similar for 95%. *KSVZ* denotes reweighted results from [20], *DFSZ* results from this paper. Both are combined with equal probability for the case *Combined*. The combination only considering models with DW number of unity is shown as $N_{\mathrm{DW}} = 1$.

$|\mathcal{C}_{a\gamma}|$			68% band		95% band	
One-sided limit	68%	95%	16%	84%	2.5%	97.5%
KSVZ	0.833	0.135	4.684	0.427	15.274	0.068
DFSZ	0.809	0.164	4.529	0.482	19.272	0.08
Combined	0.819	0.148	4.593	0.451	17.285	0.074
$N_{\mathrm{DW}} = 1$	5.294	0.769	22.773	2.733	36.729	0.731

$N_{\mathrm{DW}} = 1$ a significant percentage of models is above $\log |\mathcal{C}_{a\gamma}| \gtrsim 1.5$. The lines of $E/N = 2/3$ and $E/N = 8/3$ are clearly visible for DFSZ-type models, but also for KSVZ-type models. The relative difference between the 68% limits of KSVZ[3]- and DFSZ-type axions is only ~3% and ~19% for the 95% limits with the DFSZ limit being higher in the latter case. Taking into account possible effects from diverging theory assumptions, this relative difference can be seen as negligible.

While the investigation of different theoretical assumptions is beyond the scope of this paper, note that other assumptions on the full set of models only modify the relative importance of the prominent $DFSZ_2$ and $DFSZ_3$ peaks. Consider, for example, a different definition of multiplicity based on minimal potentials. This dramatically increases their probability mass but does not shift the overall cumulative probability to higher or lower $|\mathcal{C}_{a\gamma}|$ values. In this sense, any variation of theoretical assumptions (excluding model selection criteria) should lie between the cumulative probabilities of the $n_D = 2$ and continuum cases.

Translating these limits to $g_{a\gamma}$ over a range of axion masses, we obtain Fig. 8 (top). An experimental exclusion limit touching the 68% line excludes 68% of the probability mass over the model space under the assumptions outlined above given a specific mass range. An experiment targeting sensitivity down to the 95% line will be sensitive to 95% of the probability for all models in the targeted mass range. We include these and the 99% limit for DFSZ-type as well as KSVZ-type models and the combined case of $N_{\mathrm{DW}} = 1$. In black, we also include the maximal $\widehat{E/N}$ value we found for $DFSZ_9$. In addition to being excluded by experiments for a large fraction of the m_a range, this model may likely also be subject to phenomenological constraints (see Sec. II D).

With this work, it is now possible for the first time to give values of one-sided limits or axion bands for the combined KSVZ and DFSZ case, assuming a DFSZ-type axion to be equally likely as a KSVZ-type one. The associated PDF for the combined "all N_{DW}"-case is shown in Fig. 7. In $\log |\mathcal{C}_{a\gamma}|$-space with the relatively course binning chosen, the distributions look roughly Gaussian with the exception of several notable peaks, at $E/N = 5/3, 8/3, 2/3, 14/3$, and $-4/3$ (from left to right). Note, however, that the true underlying distribution is comprised out of a multitude of delta peaks, and thus, is fundamentally discrete. Central 68% and 95% bands from this distribution are used in Fig. 8 (bottom) together with a previous estimate for the same band from [19]. Previous work was either limited to very few extensions of DFSZ-type [19] or the KSVZ case [20]. Even now, many caveats have to be kept in mind, like the imprecise prediction for $DFSZ_8$ and $DFSZ_9$ models or the lack of selection criteria in the DFSZ case. Acknowledging this, we nevertheless deem it useful to provide usable data of typical limits and bands for a variety of scenarios. An overview can be found in Table IV, and more detailed information is hosted on the website "zenodo" together with the model catalogs (see end of Sec. V for links).

V. SUMMARY AND OUTLOOK

The PQ mechanism is the most commonly considered solution to the strong CP problem, and the appearing Goldstone boson, the axion, is one of the most promising dark matter candidates. While the axion solves the strong CP problem in a model independent way, its low-energy couplings depend on UV-models. With the booming axion experimental program, an identification of all these models within the two large classes of invisible axion models and the extraction of predictions for experiments are of high importance. In this work, we have systematically calculated the axion-photon coupling for a large number of DFSZ-type models. We give limits that have to be reached in order to be sensitive to a certain fraction of the probability mass of these models.

We have started by discussing (phenomenological) selection criteria, such as the absence of FCNCs and the DW problem, to extract preferred DFSZ-type models. In contrast to the KSVZ axions, where all selection criteria follow from cosmological bounds on additional fermions, for DFSZ-type axions we have not find criteria with a sufficient level of generality, merely desirable features.

Next, we have put forth a recipe for calculating all anomaly ratios and hence all axion-photon couplings. This recipe is based on the fact that the PQ charges are not free but fixed by linear consistency and phenomenology relations. For the sake of calculating the anomaly ratio, this reduces the procedure of DFSZ-type model building to solving LSEs. Thus, systematically going through all Yukawa sectors and solving all possible LSEs for each,

---

[3]Again, considering all *preferred* KSVZ-type models, see [20] for more information.

we have derived all possible anomaly ratios for up to seven Higgs doublets.

In addition, by counting how many models lead to a certain anomaly ratio and establishing relative probabilities of these models, we have been able to assign probabilities to each anomaly ratio. For this counting of models, we have considered as a model the Lagrangian that arises by combining different potentials that give rise to the same set of PQ charges and by adding the Yukawa couplings compatible with the resulting set of PQ charges. In this way, we have taken into account the general mantra that all terms allowed by symmetry should be included and avoid overcounting.

The resulting anomaly ratio distributions have their median at $E/N = 5/3$, their maximum values at $E/N = 2/3$ and $E/N = 8/3$, and a characteristic shape that is similar to the one of KSVZ-type models. We have explained these observations by thinking of the resulting sets of PQ charges as discrete charge distributions with uniform probability and symmetry around zero.

While, in principle, our recipe works for an arbitrary number of Higgs doublets, the necessary computational time becomes too large for eight or more doublets. Simple sampling of potential terms leads to a significant bias, so that we have constructed estimates for $n_D > 7$ based on the expected smoothness of the distributions. Moreover, by using an incremental construction procedure, we have been able to find a maximal anomaly ratio that is more than a factor of 2 higher than in previous estimates [19].

Regarding the axion experimental program, the anomaly ratio distributions confirm the experimental importance of the values dictated by the minimal DFSZ models, namely $E/N = 2/3$ and $E/N = 8/3$, since they are also favored for every number of Higgs doublets (except $n_D = 3$ with the Weinberg-Glashow-Paschos condition imposed). However, it also shows that plenty of viable parameter space lies above and below these lines. Overall, this means that a nonobservation at these favored values is not enough to declare the axion excluded, while an observation above these values would be a hint for more than one additional Higgs doublet from the DFSZ-type point of view. The statistical interpretation also reveals that both KSVZ and DFSZ models set very similar sensitivity requirements on experiments.

For $n_D \geq 4$, we have found a subset of models with DW number $N_{\mathrm{DW}} = 1$, making DFSZ-type models theoretically more viable in postinflationary scenarios. This subset even displays a significantly enhanced axion-photon coupling compared to the minimal scenarios for both invisible axion classes, hence making these models on average easier to probe.

Our analysis can be extended in multiple directions. For instance, it would be interesting to perform a similar analysis for models with a right-handed neutrino or KSVZ and DFSZ hybrid models, namely models with additional Higgs singlets, Higgs doublets, and heavy quarks. From our arguments regarding the anomaly ratio from a mathematical point of view, even though Eq. (13) would change, we expect a similar shape of the resulting distributions and axion mass versus axion-photon coupling exclusion lines. This expectation does, however, not make an explicit analysis dispensable. Furthermore, it would be interesting to investigate other axion couplings, such as the axion-electron coupling. While the other couplings depend on the VEVs of the Higgs doublets, which makes the parameter space higher dimensional, the perturbative range of the top and bottom Yukawa couplings [95] or phenomenological constraints could be used to give reasonable limits. Additionally, it would be desirable to find a better estimate for the anomaly distribution of eight or more doublets, or even an unbiased way to calculate it.

Finally, it is interesting to mention that with the identification and classification of both large classes of invisible axion models, also a comparison with other classes of axion models is possible. For instance, there exists the two-form implementation of the QCD axion [8,96,97]. This intrinsically is a gauge formulation of the axion, and as such, no explicit PQ violating processes are possible. This is not true for the ordinary invisible axion. Hence, should the axion be detected, PQ violating processes represent an interesting feature to not only distinguish the two-form axion from the ordinary invisible axion but to completely eliminate it.

Lastly, it should be said that our analysis is useful for axion searches irrespective of the statistical interpretation. By providing all possible E/N values for up to seven doublets and a full catalog for up to five doublets, in the case of a detection, one can proceed to do hypothesis testing with the compatible models. Since all E/N values for preferred KSVZ models are also known, this could be used for the purpose of model comparison between these two model classes.

Hence, with or without a statistical perspective, our work presents another step forward in the understanding and mapping of the landscape of axion models.

[1] J. M. Pendlebury, Revised experimental upper limit on the electric dipole moment of the neutron, Phys. Rev. D **92,** 092003 (2015).

[2] S. Weinberg, *The Quantum Theory of Fields. Vol. 2: Modern Applications* (Cambridge University Press, United Kingdom, 1996), p. 489.

[3] J. Ellis and M. K. Gaillard, Strong and weak *CP* violation, Nucl. Phys. **B150,** 141 (1979).

[4] G. Dvali and C. Gomez, Quantum compositeness of gravity: Black holes, AdS and inflation, J. Cosmol. Astropart. Phys. 01 (2014) 023.

[5] G. Dvali, C. Gomez, and S. Zell, Quantum breaking bound on de Sitter and swampland, Fortschr. Phys. **67,** 1800094 (2019).

[6] G. Dvali, *S*-matrix and anomaly of de Sitter, Symmetry **13,** 3 (2020).

[7] G. Dvali, C. Gomez, and S. Zell, A proof of the axion?, arXiv:1811.03079.

[8] G. Dvali, Strong-*CP* with and without gravity, arXiv:2209 .14219.

[9] R. D. Peccei and H. R. Quinn, CP Conservation in the Presence of Pseudoparticles, Phys. Rev. Lett. **38,** 1440 (1977).

[10] R. D. Peccei and H. R. Quinn, Constraints imposed by CP conservation in the presence of pseudoparticles, Phys. Rev. D **16,** 1791 (1977).

[11] S. Weinberg, A New Light Boson?, Phys. Rev. Lett. **40,** 223 (1978).

[12] F. Wilczek, Problem of Strong *P* and *T* Invariance in the Presence of Instantons, Phys. Rev. Lett. **40,** 279 (1978).

[13] M. Srednicki, Axion couplings to matter: (I). *CP*-conserving parts, Nucl. Phys. **B260,** 689 (1985).

[14] A. R. Zhitnitsky, On possible suppression of the axion hadron interactions. (In Russian), Sov. J. Nucl. Phys. **31,** 260 (1980).

[15] M. Dine, W. Fischler, and M. Srednicki, A simple solution to the strong *CP* problem with a harmless axion, Phys. Lett. **104B,** 199 (1981).

[16] J. E. Kim, Weak Interaction Singlet and Strong *CP* Invariance, Phys. Rev. Lett. **43,** 103 (1979).

[17] M. A. Shifman, A. I. Vainshtein, and V. I. Zakharov, Can confinement ensure natural *CP* invariance of strong interactions?, Nucl. Phys. **B166,** 493 (1980).

[18] L. Di Luzio, M. Giannotti, E. Nardi, and L. Visinelli, The landscape of QCD axion models, Phys. Rep. **870,** 1 (2020).

[19] L. Di Luzio, F. Mescia, and E. Nardi, Window for preferred axion models, Phys. Rev. D **96,** 075003 (2017).

[20] V. Plakkot and S. Hoof, Anomaly ratio distributions of hadronic axion models with multiple heavy quarks, Phys. Rev. D **104,** 075017 (2021).

[21] G. Grilli di Cortona, E. Hardy, J. Pardo Vega, and G. Villadoro, The QCD axion, precisely, J. High Energy Phys. 01 (2016) 034.

[22] G. 't Hooft, How instantons solve the u(1) problem, Phys. Rep. **142,** 357 (1986).

[23] C. G. Callan, R. Dashen, and D. J. Gross, Toward a theory of the strong interactions, Phys. Rev. D **17,** 2717 (1978).

[24] A. Ernst, A. Ringwald, and C. Tamarit, axion predictions in $SO(10) \times U(1)_{PQ}$ models, J. High Energy Phys. 02 (2018) 103.

[25] D. J. Gross, R. D. Pisarski, and L. G. Yaffe, QCD and instantons at finite temperature, Rev. Mod. Phys. **53,** 43 (1981).

[26] P. Sikivie, Axions, Domain Walls, and the Early Universe, Phys. Rev. Lett. **48,** 1156 (1982).

[27] A. Vilenkin and E. P. S. Shellard, *Cosmic Strings and Other Topological Defects* (Cambridge University Press, Cambridge, England, 2000), p. 7.

[28] G. R. Dvali and G. Senjanovic, Is There a Domain Wall Problem?, Phys. Rev. Lett. **74,** 5178 (1995).

[29] G. Lazarides and Q. Shafi, Axion models with no domain wall problem, Phys. Lett. **115B,** 21 (1982).

[30] A. Pich, Flavor physics and *CP* violation, in *6th CERN-Latin-American School of High-Energy Physics* (2013), pp. 119–144, arXiv:1112.4094.

[31] I. P. Ivanov, Building and testing models with extended Higgs sectors, Prog. Part. Nucl. Phys. **95,** 160 (2017).

[32] S. L. Glashow and S. Weinberg, Natural conservation laws for neutral currents, Phys. Rev. D **15,** 1958 (1977).

[33] E. A. Paschos, Diagonal neutral currents, Phys. Rev. D **15,** 1966 (1977).

[34] M. Y. Gogberashvili and G. R. Dvali, Hierarchy at Yukawa constants and K0 anti-K0, B0 anti-B0 oscillations in the model with two Higgs doublets. (In Russian), Sov. J. Nucl. Phys. **53,** 491 (1991).

[35] A. Pich and P. Tuzon, Yukawa alignment in the two-Higgs-doublet model, Phys. Rev. D **80,** 091702 (2009).

[36] I. de Medeiros Varzielas and J. Talbert, FCNC-free multi-Higgs-doublet models from broken family symmetries, Phys. Lett. B **800,** 135091 (2020).

[37] T. P. Cheng and M. Sher, Mass-matrix ansatz and flavor nonconservation in models with multiple Higgs doublets, Phys. Rev. D **35,** 3484 (1987).

[38] S. Carrolo, J. C. Romão, J. P. Silva, and F. Vazão, Symmetry and decoupling in multi-Higgs boson models, Phys. Rev. D **103,** 075026 (2021).

[39] A. Peñuelas and A. Pich, flavor alignment in multi-Higgs-Doublet models, J. High Energy Phys. 12 (2017) 084.

[40] M. Farina, D. Pappadopulo, F. Rompineve, and A. Tesi, The photo-philic QCD axion, J. High Energy Phys. 01 (2017) 095.

[41] J. Bezanson, S. Karpinski, V. B. Shah, and A. Edelman, Julia: A fast dynamic language for technical computing, arXiv: 1209.5145.

[42] StaticArrays.jl (2022), https://juliaarrays.github.io/ StaticArrays.jl/.

[43] K. Pearson, IX. Mathematical contributions to the theory of evolution.—XIX. Second supplement to a memoir on skew variation, Phil. Trans. R. Soc. A **216,** 429 (1916).

[44] J. Sloan, M. Hotz, C. Boutan *et al.*, Limits on axion–photon coupling or on local axion density: Dependence on models of the milky way's dark halo, Phys. Dark Universe **14,** 95 (2016).

[45] V. Anastassopoulos, F. Avignone, A. Bykov *et al.*, Toward a medium-scale axion helioscope and haloscope, J. Instrum. **12,** P11019 (2017).

[46] S. Scopel, Particle dark matter candidates, J. Phys. Conf. Ser. **120,** 042003 (2008).

[47] I. Shilon, A. Dudarev, H. Silva, and H. H. J. ten Kate, Conceptual design of a new large superconducting toroid for

IAXO, the New International AXion Observatory, IEEE Trans. Appl. Supercond. **23,** 4500604 (2013).

[48] CAST Collaboration, New CAST limit on the axion-photon interaction, Nat. Phys. **13,** 584 (2017).

[49] E. Armengaud, D. Attié, S. Basso *et al.*, Physics potential of the International Axion Observatory (IAXO), J. Cosmol. Astropart. Phys. 06 (2019) 047.

[50] S. Beurthey *et al.*, MADMAX status report, arXiv:2003 .10894.

[51] T. Grenet, R. Ballou, Q. Basto *et al.*, The grenoble axion haloscope platform (GrAHal): Development plan and first results, arXiv:2110.14406.

[52] A. A. Melcón *et al.* (CAST Collaboration), First results of the CAST-RADES haloscope search for axions at 34.67 μeV, J. High Energy Phys. 10 (2020) 075.

[53] N. Crisosto, P. Sikivie, N. S. Sullivan, D. B. Tanner, J. Yang, and G. Rybka, ADMX SLIC: Results from a Superconducting *LC* Circuit Investigating Cold Axions, Phys. Rev. Lett. **124,** 241101 (2020).

[54] J. A. Devlin *et al.*, Constraints on the Coupling between Axionlike Dark Matter and Photons Using an Antiproton Superconducting Tuned Detection Circuit in a Cryogenic Penning Trap, Phys. Rev. Lett. **126,** 041301 (2021).

[55] N. Crescini *et al.* (QUAX Collaboration), Axion Search with a Quantum-Limited Ferromagnetic Haloscope, Phys. Rev. Lett. **124,** 171801 (2020).

[56] D. Alesini *et al.*, Galactic axions search with a superconducting resonant cavity, Phys. Rev. D **99,** 101101 (2019).

[57] D. Alesini *et al.*, Search for invisible axion dark matter of mass $m_a = 43$ μeV with the QUAX–$a\gamma$ experiment, Phys. Rev. D **103,** 102004 (2021).

[58] C. A. Thomson, B. T. McAllister, M. Goryachev, E. N. Ivanov, and M. E. Tobar, Upconversion Loop Oscillator Axion Detection Experiment: A Precision Frequency Interferometric Axion Dark Matter Search with a Cylindrical Microwave Cavity, Phys. Rev. Lett. **126,** 081803 (2021); **127,** 019901(E) (2021).

[59] B. T. McAllister, G. Flower, E. N. Ivanov, M. Goryachev, J. Bourhill, and M. E. Tobar, The ORGAN experiment: An axion haloscope above 15 GHz, Phys. Dark Universe **18,** 67 (2017).

[60] J. Jeong, S. Youn, S. Bae, J. Kim, T. Seong, J. E. Kim, and Y. K. Semertzidis, Search for Invisible Axion Dark Matter with a Multiple-Cell Haloscope, Phys. Rev. Lett. **125,** 221302 (2020).

[61] A. V. Gramolin, D. Aybas, D. Johnson, J. Adam, and A. O. Sushkov, Search for axion-like dark matter with ferromagnets, Nat. Phys. **17,** 79 (2021).

[62] C. P. Salemi *et al.*, Search for Low-Mass Axion Dark Matter with AbracaDabra-10 cm, Phys. Rev. Lett. **127,** 081801 (2021).

[63] J. L. Ouellet *et al.*, First Results from AbracaDabra-10 cm: A Search for Sub-μeV Axion Dark Matter, Phys. Rev. Lett. **122,** 121802 (2019).

[64] L. Zhong *et al.* (HAYSTAC Collaboration), Results from phase 1 of the HAYSTAC microwave cavity axion experiment, Phys. Rev. D **97,** 092001 (2018).

[65] K. M. Backes *et al.* (HAYSTAC Collaboration), A quantum-enhanced search for dark matter axions, Nature (London) **590,** 238 (2021).

[66] C. Hagmann, P. Sikivie, N. Sullivan, and D. Tanner, Results from a search for cosmic axions, Phys. Rev. D **42,** 1297 (1990).

[67] S. DePanfilis, A. Melissinos, B. Moskowitz, J. T. Rogers, Y. K. Semertzidis, W. U. Wuensch, H. J. Halama, A. G. Prodell, W. B. Fowler, and F. A. Nezrick, Limits on the Abundance and Coupling of Cosmic Axions at $4.5 < m_a < 5.0$ μeV, Phys. Rev. Lett. **59,** 839 (1987).

[68] N. Du *et al.* (ADMX Collaboration), A Search for Invisible Axion Dark Matter with the Axion Dark Matter Experiment, Phys. Rev. Lett. **120,** 151301 (2018).

[69] T. Braine *et al.* (ADMX Collaboration), Extended Search for the Invisible Axion with the Axion Dark Matter Experiment, Phys. Rev. Lett. **124,** 101303 (2020).

[70] C. Bartram *et al.* (ADMX Collaboration), Search for Invisible Axion Dark Matter in the 3.3–4.2 μeV Mass Range, Phys. Rev. Lett. **127,** 261803 (2021).

[71] M. Baryakhtar, J. Huang, and R. Lasenby, Axion and hidden photon dark matter detection with multilayer optical haloscopes, Phys. Rev. D **98,** 035006 (2018).

[72] Y. Michimura, Y. Oshima, T. Watanabe, T. Kawasaki, H. Takeda, M. Ando, K. Nagano, I. Obata, and T. Fujita, DANCE: Dark matter axion search with riNg cavity experiment, J. Phys. Conf. Ser. **1468,** 012032 (2020).

[73] B. Aja *et al.*, The Canfranc Axion Detection Experiment (CADEx): Search for axions at 90 GHz with kinetic inductance detectors, J. Cosmol. Astropart. Phys. 11 (2022) 044.

[74] J. Liu *et al.* (BREAD Collaboration), Broadband Solenoidal Haloscope for Terahertz Axion Detection, Phys. Rev. Lett. **128,** 131801 (2022).

[75] A. J. Millar *et al.*, ALPHA: Searching For dark matter with plasma haloscopes, arXiv:2210.00017.

[76] M. Lawson, A. J. Millar, M. Pancaldi, E. Vitagliano, and F. Wilczek, Tunable Axion Plasma Haloscopes, Phys. Rev. Lett. **123,** 141802 (2019).

[77] H. Chang *et al.* (TASEH Collaboration), First Results from the Taiwan Axion Search Experiment with a Haloscope at 19.6 μeV, Phys. Rev. Lett. **129,** 111802 (2022).

[78] D. Alesini, D. Babusci, C. Braggio *et al.*, Search for Galactic axions with a high-Q dielectric cavity, Phys. Rev. D **106,** 052007 (2022).

[79] A. P. Quiskamp, B. T. McAllister, P. Altin *et al.*, Direct search for dark matter axions excluding ALP cogenesis in the 63–67 micro-eV range, with The ORGAN experiment, arXiv:2203.12152.

[80] M. J. Jewell, A. F. Leder *et al.* (HAYSTAC Collaboration), New results from HAYSTAC's phase II operation with a squeezed state receiver, arXiv:2301.09721.

[81] S. Lee, S. Ahn, J. Choi, B. R. Ko, and Y. K. Semertzidis, Axion Dark Matter Search around 6.7 μeV, Phys. Rev. Lett. **124,** 101802 (2020).

[82] O. Kwon, D. Lee, W. Chung *et al.*, First Results from an Axion Haloscope at CAPP around 10.7 μeV, Phys. Rev. Lett. **126,** 191802 (2021).

[83] Y. Lee, B. Yang, H. Yoon, M. Ahn, H. Park, B. Min, D. Kim, and J. Yoo, Searching for Invisible Axion Dark Matter with an 18 T Magnet Haloscope, Phys. Rev. Lett. **128,** 241805 (2022).

[84] J. Kim, O. Kwon, Ç. Kutlu *et al.*, Near-quantum-noise axion dark matter search at CAPP around 9.5 μeV, arXiv:2207 .13597.

[85] A. K. Yi, S. Ahn, Ç. Kutlu *et al.*, Axion dark matter search around 4.55 μeV with Dine-Fischler-Srednicki-Zhitnitskii sensitivity, arXiv:2210.10961.

[86] A. Berlin, R. T. D'Agnolo, S. A. R. Ellis, and K. Zhou, Heterodyne broadband detection of axion dark matter, Phys. Rev. D **104,** L111701 (2021).

[87] L. Brouwer *et al.* (DMRadio Collaboration), Projected sensitivity of DMRadio-m^3: A search for the QCD axion below 1 μeV, Phys. Rev. D **106,** 103008 (2022).

[88] D. Alesini, D. Babusci, D. Di Gioacchino *et al.*, The KLASH proposal, arXiv:1707.06010.

[89] Z. Zhang, D. Horns, and O. Ghosh, Search for dark matter with an LC circuit, Phys. Rev. D **106,** 023003 (2022).

[90] K. Nagano, T. Fujita, Y. Michimura, and I. Obata, Axion Dark Matter Search with Interferometric Gravitational Wave Detectors, Phys. Rev. Lett. **123,** 111301 (2019).

[91] H. Liu, B. D. Elwood, M. Evans, and J. Thaler, Searching for axion dark matter with birefringent cavities, Phys. Rev. D **100,** 023548 (2019).

[92] J. Schütte-Engel, D. J. E. Marsh, A. J. Millar, A. Sekine, F. Chadha-Day, S. Hoof, M. N. Ali, K. Chung Fong, E. Hardy, and L. Šmejkal, Axion quasiparticles for axion dark matter detection, J. Cosmol. Astropart. Phys. 08 (2021) 066.

[93] D. J. E. Marsh, K.-C. Fong, E. W. Lentz, L. Šmejkal, and M. N. Ali, Proposal to Detect Dark Matter using Axionic Topological Antiferromagnets, Phys. Rev. Lett. **123,** 121601 (2019).

[94] C. O'Hare, cajohare/axionlimits: Axionlimits, https:// cajohare.github.io/AxionLimits/ (2023).

[95] F. Björkeroth, L. Di Luzio, F. Mescia, E. Nardi, P. Panci, and R. Ziegler, Axion-electron decoupling in nucleophobic axion models, Phys. Rev. D **101,** 035027 (2020).

[96] G. Dvali, Three-form gauging of axion symmetries and gravity, arXiv:hep-th/0507215.

[97] O. Sakhelashvili, Consistency of the dual formulation of axion solutions to the strong *CP* problem, Phys. Rev. D **105,** 085020 (2022).